

Research paper

Impact of sequence stratigraphy, depositional facies, diagenesis and CO₂ charge on reservoir quality of the lower cretaceous Quantou Formation, Southern Songliao Basin, China



Zheng Cao^a, Chengyan Lin^{a,*}, Chunmei Dong^a, Lihua Ren^a, Shuo Han^a, Junjie Dai^a, Xiao Xu^b, Mingyang Qin^c, Peng Zhu^d

^a School of Geosciences, China University of Petroleum, Qingdao, Shandong, 266580, China

^b The Twelfth Oil Production Factory, Changqing Oil Field, Xi'an, 710000, China

^c School of Geosciences and Info-Physics Engineering, Central South University, Changsha, 410083, China

^d College of Energy Resources, Chengdu University of Technology, Chengdu, 610059, China

ARTICLE INFO

Keywords:

Reservoir quality
Sequence stratigraphic framework
Depositional facies
Diagenesis
CO₂ charging
Songliao basin

ABSTRACT

The fourth member of the Lower Cretaceous Quantou Formation in Southern Fuxin Uplift zone of the Southern Songliao Basin is typical tight oil reservoir which has recently been explored and produced. For effective exploration and development, the evaluation and control factors of the reservoir quality of the K₁q₄ sandstones should be thoroughly studied. The study focused on the control of the combination of sequence stratigraphy, depositional facies and diagenesis on the reservoir quality, and identified the impact of CO₂ charging, based on the core and thin section observation, XRD, SEM, fluid inclusion and isotope testing and analysis. The fourth member of the Lower Cretaceous Quantou Formation consists of lowstand system tracts (LST), transgressive system tracts (TST) and highstand system tracts (HST). The K₁q₄ sandstones were mostly deposited in distributary channels and crevasse splays of a delta plain within the LST and TST, and underwater distributary channels and sheet sands of a delta front within the HST. The K₁q₄ sandstones, mostly silt to medium grained, medium to well sorted, and are mostly lithic arkoses and feldspathic litharenites, have undergone significantly diagenetic alterations, such as compaction, quartz cementation, unstable grains (feldspar and volcanic fragments) dissolution, carbonate cementation and clay minerals cementation. The reservoir quality of the K₁q₄ sandstones are poor with low porosity and permeability, showing variations among the different system tracts and depositional facies, and are influenced by the charging of CO₂ and controlled by the combination of sequence stratigraphy, depositional facies and diagenesis. The sandstones with high reservoir quality are mostly deposited in high energy environments, including the (underwater) distributary channel sandstones, especially the LST distributary channel sandstones with the best reservoir quality among the LST, TST and HST sandstones, which can be ascribed to larger grain size and better sorting resulting in larger intergranular pore space after compaction, and less content of carbonate cements, illite and mixed-layer I/S, and more pore-lining chlorite and more effectively dissolution. The poor reservoir quality of sandstones from crevasse splay and sheet sand is due to the small grain size and bad sorting which resulted in extensive compaction and the resulting weak dissolution. The charging of CO₂ has dual impact on the reservoir quality of the K₁q₄ sandstones. The CO₂ charging can induce the dissolution of unstable detrital grains and the precipitation of dawsonite. The former create new secondary pore space, while the latter occupy the intergranular pore space. The CO₂ charging is harmful to the reservoir quality when the dawsonite content exceeds a threshold of 5%.

1. Introduction

Volumetrically significant tight oil resources have been discovered and explored in the fourth member of Lower Cretaceous Quantou formation sandstones in Southern Fuxin Uplift zone, Southern Songliao

Basin located on the northeastern China plate (Fig. 1). The sandstone reservoirs of the fourth member of Quantou formation (K₁q₄) lay beneath the hydrocarbon source rock of the first member of Qingshankou formation, which makes the K₁q₄ reservoirs oil rich. The K₁q₄ reservoirs in the study area are generally buried less than 2000 m, and are of low

* Corresponding author.

E-mail address: ycdzycms2017@126.com (C. Lin).

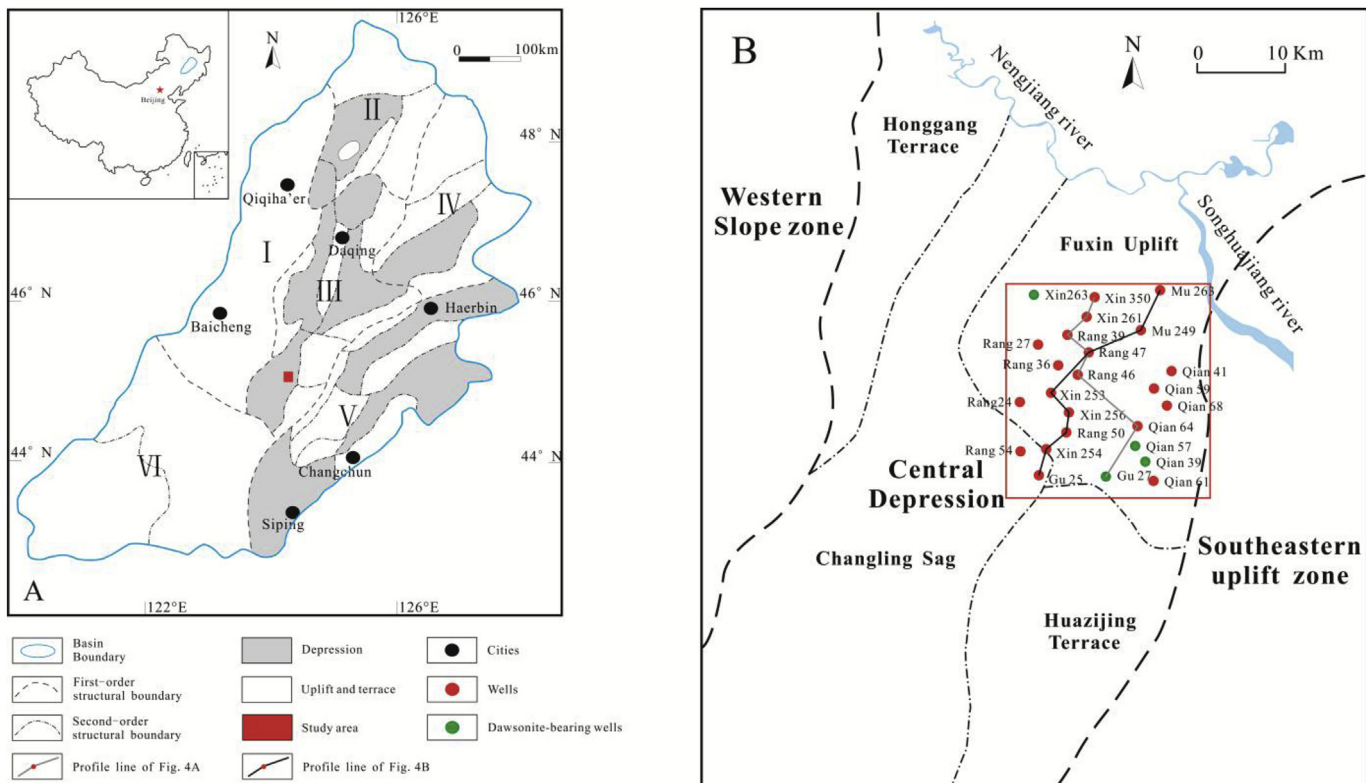


Fig. 1. (A) Location map of the study area and sub-tectonic units of the Songliao Basin (I) Western Slope Zone, (II) Northern Plunge Zone, (III) Central Depression Zone, (IV) Northeastern Uplift Zone, (V) Southeastern Uplift Zone, (VI) Southwestern Uplift Zone (modified from Feng et al., 2010; Xi et al., 2015a,b); (B) the sub-tectonic units of the study area and well locations (modified from Xi et al., 2015a,b).

permeability with characteristics of strong reservoir heterogeneity, which makes that the reservoir deliverability within adjacent exploration well-areas shows large differences with evidence from drilling practices. To decrease the exploration risk and improve the reservoir deliverability, it is urgent to make a thorough understanding of control factors of the reservoir quality of the K_1q_4 sandstone reservoirs.

Sequence stratigraphy, depositional facies and diagenesis can exert a strong control on the reservoir quality, which has attracted the attention of substantial research (e.g., Morad et al., 2010; Trendell et al., 2012; Li et al., 2013; Amel et al., 2015; Marchand et al., 2015; Lan et al., 2016). Although there are many publications concentrated on sequence stratigraphy, depositional facies and diagenesis in the southern Songliao basin respectively, little attention has been paid to the combination of them on how they impact the reservoir quality (Li et al., 2007; Hu et al., 2008; Xiong et al., 2008; Feng et al., 2013; Li et al., 2013; Xi et al., 2015a,b). Former studies on the study area mainly concentrate on how depositional facies or diagenesis control the reservoir quality, ignoring the influence of sequence stratigraphy on the distribution of depositional facies and the variations of diagenetic alterations within different system tracts and depositional facies. The deposition facies within sequence stratigraphic framework is the key factor controlling the primary porosity and permeability of sandstones, sand body geometry and architecture, pore-water chemistry, and spatial and temporal distribution of early diagenetic alteration (Morad et al., 2000; Kim et al., 2007; Hammer et al., 2010). The tight sandstones generally undergone complicated diagenetic alterations, which exerted significant control on the reservoir quality (Karim et al., 2010; Yang et al., 2012; Zhang et al., 2015).

In this article, we link deposition facies and diagenetic alterations to the sequence stratigraphy framework to identify how they affect the reservoir quality in the study area, with integration of core descriptions, casting thin-section, X-ray diffractions and scanning electron microscope analyses. The result of this study demonstrates the impact of

depositional facies and diagenesis within sequence stratigraphy framework, as well as CO_2 charging, on the reservoir quality and heterogeneity, which can provide a tool for reservoir prediction in tight sandstones in this area and references for other tight sandstones with similar geological background.

2. Geological setting

Songliao basin, a large scale Mesozoic-Tertiary depositional basin on the northeast China plate, can be divided into the northern and southern parts due to the different tectonic subsidence history (Wei et al., 2010), and consists of six first order tectonic zones: west slope zone, northern plunge zone, central depression zone, southeast uplift zone, southeastern uplift zone and southwestern uplift zone (Fig. 1). Central depression zone is the main oil producing province which covers 4 secondary order tectonic units on the southern Songliao basin: Honggang terrace, Changling sag, Huazijing terrace, and Fuxin uplift. The study area located on the southern Fuxin uplift zone and covers an area of 1200 km^2 (Fig. 1).

The tectonic evolution of southern Songliao basin experienced four stages: the mantle upwelling stage, the rift stage, the post-rift stage and structural inversion stage (Feng et al., 2010). The mantle upwelling occurred during the Late Jurassic, and Huoshiling (K_1h) formation is deposited during the stage, which is characterized by volcaniclastic and pyroclastic rocks. The rifting stage occurred during the sedimentary period of the Lower Cretaceous Shahezi (K_1sh), Yingcheng (K_1yc), and Denglouku (K_1d) formations, which is characterized by alluvial fan, fan delta, fluvial, deltaic, and lacustrine clastic sediments. Fine grained sandstones, silt sandstones, and mudstones deposited in fluvial-delta and lacustrine environment constituted the Lower Cretaceous Quantou (K_1q) Formation. The Upper Cretaceous Qingshankou (K_2qn), Yaojia (K_2y), and Nengjiang (K_2n) formations sediments (post-rift tectonic stratigraphic unit) are characterized by the delta and deep lake

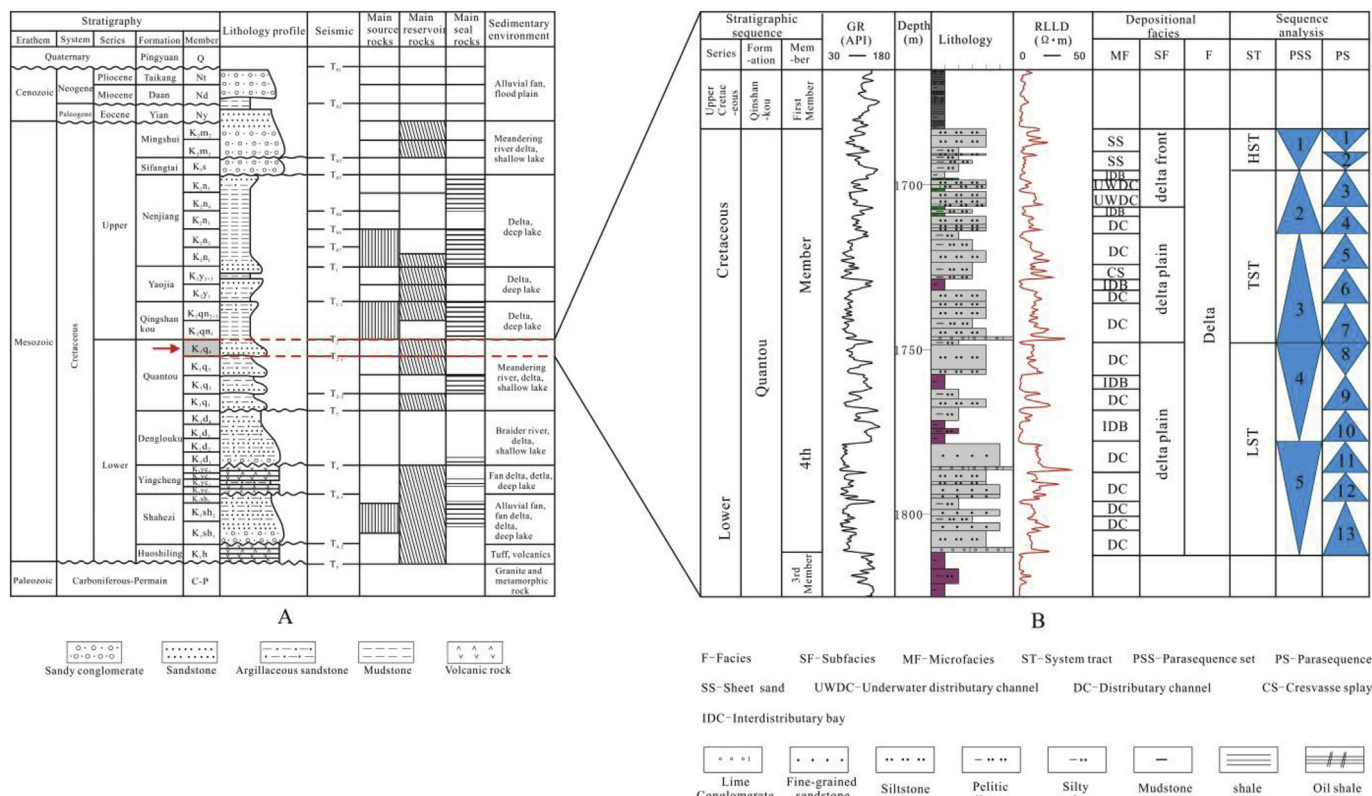


Fig. 2. (A) Generalized Mesozoic-Quaternary stratigraphy of the Songliao Basin, showing major source-reservoir-caprock combinations (modified from Xi et al., 2015a,b); (B) Representative stratigraphic column of the Early Cretaceous Quantou Formation in the study area of the southern Songliao basin, showing the depositional facies and system tracts. LST - lowstand systems tract, TST - transgressive systems tract, and HST – highstand systems tract.

sediments. Upper Cretaceous Sifangtai (K_{2s}) to Quaternary Pingyuan (Q) deposits (structural inversion tectonic stratigraphic unit) consist mostly of fine-grained fluvial-delta clastic sediments.

The Quantou Formation (K_{1q}) is a thick sequence of fan-deltaic and lacustrine sandstones deposited in the post-rift stage of the tectonic evolution of the southern Songliao basin, lying beneath the thick hydrocarbon source rocks of the late Cretaceous Qingshankou Formation (K_{2qn}), and the two of them formed the configuration of upper hydrocarbon source rocks and lower reservoir sandstones (Fig. 2). The studied section is the fourth member of Quantou Formation (K_{1q4}), the main oil layer in the southern Songliao basin. The source of the oil in the K_{1q4} sandstones is originated from the first member of the Qingshankou Formation (K_{2qn1}), and there are two main accumulation period in the Fuxin uplift zone. Two hydrocarbon charging started at 85–65Ma and 50–25Ma, respectively, which correspond to the Nenjiang (k_2n) period to Mingshui period, and the end of the Mingshui period to the end of the Paleogene (Zou et al., 2007).

3. Samples and methods

Rock compositions data of 212 thin sections samples, 109 bulk rock and clay fraction XRD data, 4099 reservoir porosity and permeability data, and 600 grain size analysis data were collected from the Research Institute of Petroleum Exploration & Development of the Jilin Oilfield Company, PetroChina.

According to the study aims and the constraints of collected data, samples were selected from the K_{1q4} drill cores of 14 wells in the study area, and another 52 sandstone samples of 10 wells were added and polished for thin sections, and in which 18 samples of 10 wells were selected for bulk rock and clay fraction XRD analysis. Therefore, a total of 174 thin sections of the K_{1q4} sandstones of 24 wells within a depth interval of 850–2000m were prepared for detailed petrographic

examination in this study. Thin sections were impregnated with blue or red epoxy resin to highlight the pores, and were partly stained with Alizarin Red S and K-ferricyanide for carbonate mineral determination. The modal composition of the sandstones was achieved by counting 300 points on thin sections. Point counting was performed on 20 collected thin sections to check the correctness of the collected composition data, which can provide a standard deviation of 5.5% or less. For the added sandstone samples, point counting was performed on each thin section.

The textural relationships between the authigenic minerals was identified in 14 representative sample chips that were gold-coated using a Hitachi S-4800 scanning electron microscope (SEM) under an acceleration voltage of 20 kV. 9 sandstones samples were doubly polished with thickness of approximately 100 µm for fluid inclusion petrographic analysis and microthermometric measurements. The microthermometry of fluid inclusions was measured using a Linkam THMSG 600 heating and cooling stage which enables temperatures of phase transitions in the range of -180 to 500 °C. Precision of the measured temperature for the homogenization temperature (T_h) is ± 1 °C.

16 organic matter-free sandstone samples were selected for oxygen and carbon stable isotope analyses using a Thermo-Finnigan MAT 253 isotope ratio mass spectrometer. Precision was $\pm 0.08\text{‰}$ for oxygen and $\pm 0.06\text{‰}$ for carbon. Oxygen and carbon isotope data are presented in the d notation relative to the Vienna Pee Dee Belemnite (VPDB) standards.

4. Depositional facies within sequence stratigraphic framework

The fourth member of Quantou Formation (K_{1q4}) corresponds to a third order sequence (Wang et al., 2007; Feng et al., 2010), comprising the lowstand system tract (LST), transgressive system tract (TST) and highstand system tract (HST). The bottom boundary of the K_{1q4} reservoirs is characterized by the lag deposits rich in calcareous



Fig. 3. Core photograph of the typical sedimentary structures of the K_{1q4} sandstones. (A) Parallel beddings, fine-grained sandstones, distributary channels of delta plains of the LST (well Gu27, 1232.6 m). (B) Heterogeneity of oil distribution, fine-grained sandstones with massive bedding in the lower part and the cross bedding in the upper part, distributary channels of delta plains of the LST (well Mu249, 1246.1 m). (C) Lag deposits with erosive base of distributary channels of delta plains of the LST (well Xin219, 1164.9 m). (D) Massive, siltstones, distributary channels of delta plains of the TST (well Rang36, 1710.8 m). (E) Cross beddings, siltstones, distributary channels of delta plains of the TST (well Qian48, 1208.7 m). (F) Lag deposits with erosive base of siltstones, distributary channels of delta plains of the TST (well Rang27, 1589.8 m). (G) Sandy mudstones with bioturbation, transition zones of the delta of the TST (well Mu249, 1219.6 m). (H) Heterogeneity of oil distribution, siltstones with massive bedding in the lower part and the cross bedding in the upper part, distributary channels of delta front of the HST (well Mu249, 1246.1 m). (I) Wavy cross-bedding, pelitic siltstones, sheet sand of delta front of the HST (well Rang36, 1653.6 m).

concretion, and is also an unconformity marked by the T_{2-1} seismic reflectance surface (Fig. 2). The top boundary of the K_{1q4} reservoirs is the surface of lithological discontinuity with dark grey mudstone of K_{2qn1} above the surface and greyish green or light grey mudstone and siltstone below, and is marked by the T_2 seismic reflectance surface (Fig. 2).

The LST, comprising two progradational parasequence sets 4 and 5, which can be further divided into three parasequences (8–10 and 11–13), respectively. The LTST sandstones are characterized by siltstones and fine-grained sandstones deposited in the distributary

channels of a delta plain, and small quantities of siltstones and pelitic sandstones deposited in crevasse splays which had relatively low-energy hydrodynamic conditions. Massive bedding, cross bedding and parallel bedding can be observed in the central and upper part of the sandstones from the distributary channel (Fig. 3A and B), and the thick lag deposits with erosion bases are commonly observed in the base of the channel sandstones (Fig. 3C). The mudstones and sandy mudstones deposited in the inter-distributary bays of a delta plain are purplish red or brownish red. During the period of the LST, the accommodation space was small, which resulted in the high hydrodynamic conditions

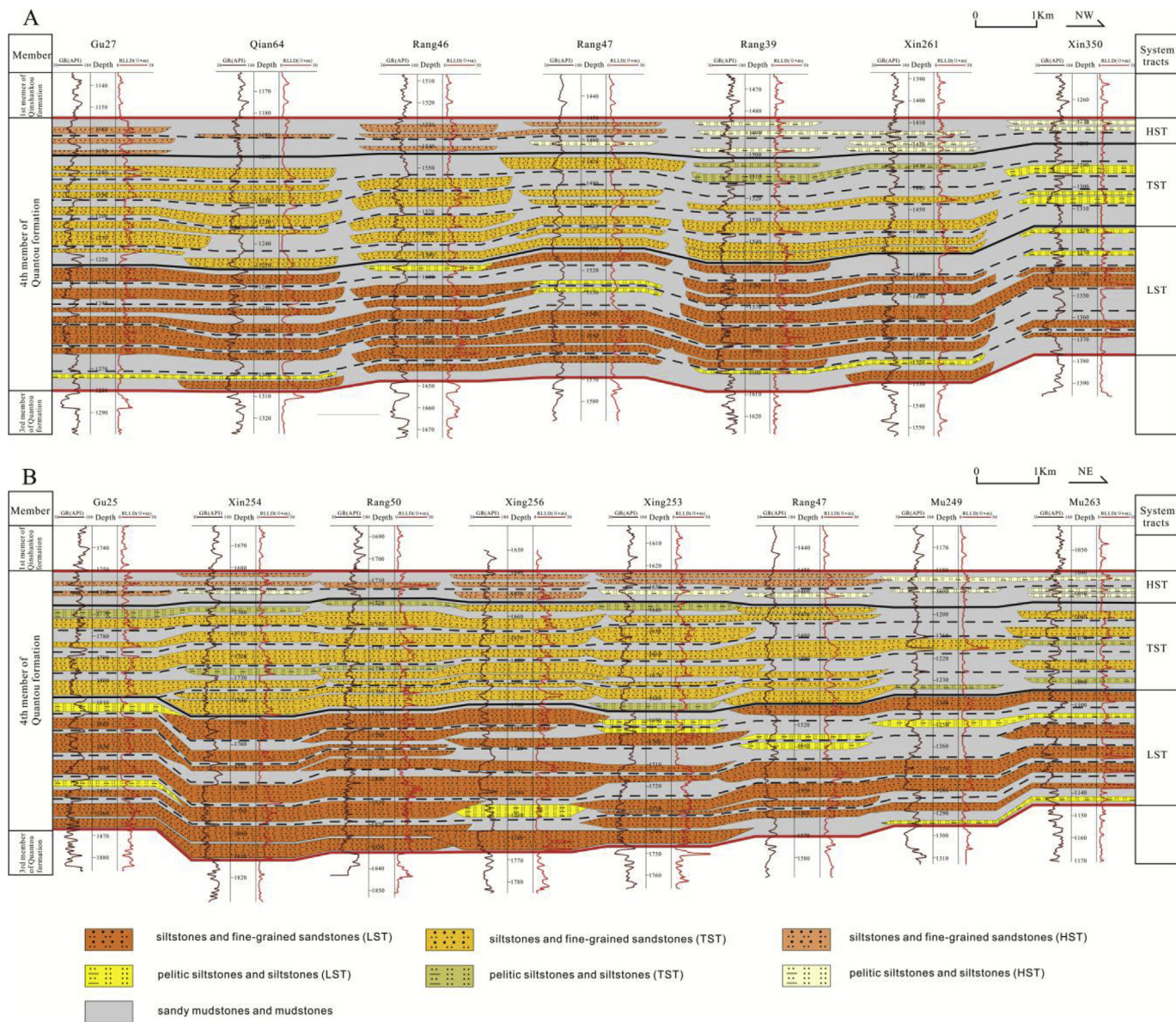


Fig. 4. Profile of the sequence stratigraphic framework of the fourth member of Quantou Formation in the study area. The profile location is labeled in Fig. 1.

and the frequent lateral amalgamation of the channel sandstones (Fig. 4). The thickness of distributary channel sandstones ranges from 2 m to 14 m (Fig. 5D, E and F), and that of the sandstones from crevasse splays is 2 m approximately.

The TST is characterized by two retrogradational parasequence set 2 (parasequence 5–7) and parasequence set 3 (parasequence 3 and 4). Accompanied by the rising of base level, the created accommodation space finally outstripped the rate of sediment supply, the parasequence started to retrograde, and the depositional facies turns from a delta plain of the early TST to a delta front of the late TST. The parasequence set 3 is comprising siltstones and fine-grained sandstones from distributary channels of a delta plain, intercalated with pelitic siltstones from crevasse splays and purplish red or brownish red mudstones from the inter-distributary bays. The parasequence set 2 is mainly made up of siltstones and fine-grained sandstones from distributary channels of the transition zone of a delta, intercalated with grey, greyish-green mudstones from inter-distributary bays. The TST distributary channel sandstones commonly have massive beddings or cross beddings with erosive bases (Fig. 3D, E and F), with thickness ranging from 2 m to 10 m, and the crevasse splay sandstones are generally less than 2 m

(Fig. 4). Mudstones or sandy mudstones from the inter-distributary bay were commonly bioturbated (Fig. 3G).

Two progradational parasequences constitute the HST. The HST is characterized by siltstones and pelitic siltstones intercalated with grey and/or dark grey mudstones. The siltstones are deposited in underwater distributary channels of a delta front, and the pelitic siltstones are mainly from sheet sand. Small cross beddings are common in the HST underwater distributary channel and sheet sand sandstones (Fig. 3H and I), and the HST sandstones are more isolated than the TST and LST sandstones (Fig. 4). During the highstand system tract, the energy of the lake increases accompanied by the base level descends, which resulted in the sheetization of distributary channel sandbodies in the delta front (Fig. 5A). The thickness of the HST underwater distributary channel sandstones ranges from 2 m to 6 m with an average of 3 m approximately, while that of the sheet sand sandstones is generally less than 2 m (Fig. 4).

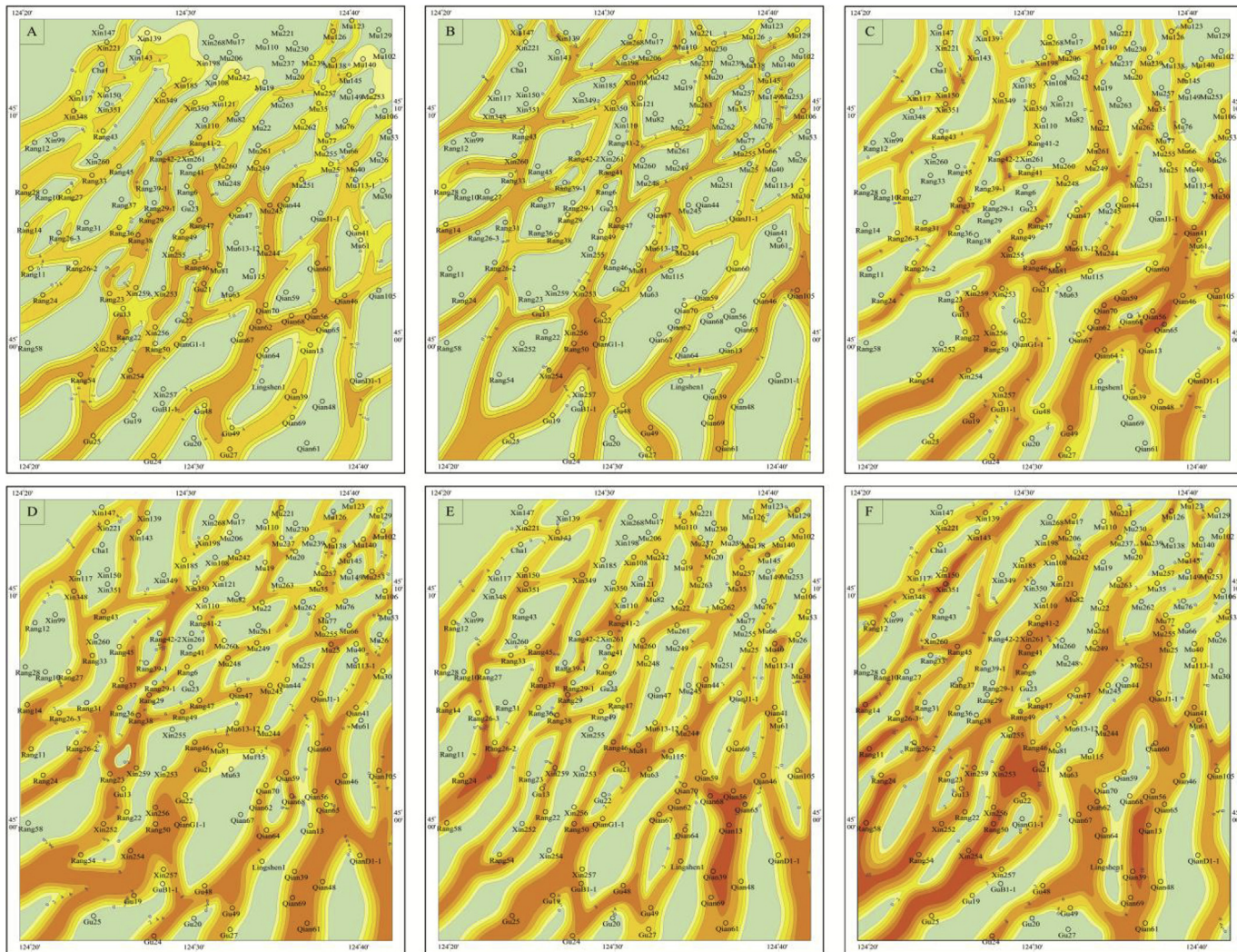


Fig. 5. Isopach map of the K₁q₄ LST (D, E, F-parasequence 8, 10, 13 respectively), TST (B and C-parasequence 3 and 5) and HST (A-parasequence 1) sandstones. The contour interval is 2 m.

5. Results

5.1. Detrital composition

The studied K₁q₄ sandstones are silt to medium grained and most of them are medium to well sorted, mainly subangular to subrounded. These sandstones are dominantly lithic arkoses and feldspathic litharenites (Fig. 6). The detrital grains are dominated by quartz ranging from 32.3% to 58.4% (av. 42.9%), in which monocrystalline quartz with characteristics of wavy extinction is dominant. The content of feldspar is 10.0%–43.2% with an average of 29.7%, which consists of plagioclase feldspar and potassium feldspar. The rock fragments content ranges from 17.0% to 45.8% with an average of 27.2%, comprising 13.1%–40.0% volcanic rock fragments with an average of 23.3%, 5.1%–18.3% metamorphic rock fragments with an average of 2.8%, and 1.0%–3.5% sedimentary rock fragments with an average of 1.6%.

5.2. Diagenetic alterations

The K₁q₄ sandstones have undergone significant diagenetic modification, and the major diagenetic alterations are compaction, quartz and carbonate cementation, growth of authigenic clay minerals and the dissolution of unstable detrital grains.

5.2.1. Compaction

Compaction of the K₁q₄ sediments resulted in deformation and rearrangement of detrital grains, and the intergranular volume (IGV) loss. Bending or deformation of ductile grains such as micas and volcanic rock fragments were also observed (Fig. 7A), which indicated an extensive mechanical compaction of K₁q₄ sandstones during burial. Chemical compaction is also observed with the existence of lineal to concavo-convex grain contacts between quartz grains (Fig. 7B).

5.2.2. Carbonate cements

Carbonate cements (0.8%–23%, av. 5.8%) in the K₁q₄ sandstones are mainly comprising ferrocalcite and ankerite, and dawsonite is only present in four wells with 43 sandstone samples in total in the study area (Fig. 1B).

Ferrocalcite and ankerite are common in the K₁q₄ sandstones (with/without dawsonite) with an average content of 1.7% and 2.3%, respectively. They both occur mainly as subhedral or euhedral crystals filling intergranular/secondary dissolution pores or as a replacement of quartz, feldspar and rock fragments (Fig. 7C andD). Moreover, ankerite engulfs or partly replaces ferrocalcite, and hence post-date ferrocalcite (Fig. 7D). Ankerite is most abundant in the TST distributary channel sandstones, while the HST underwater distributary channel sandstones have the highest average content of the ferrocalcite, compared with sandstones from other depositional facies and system tracts respectively.

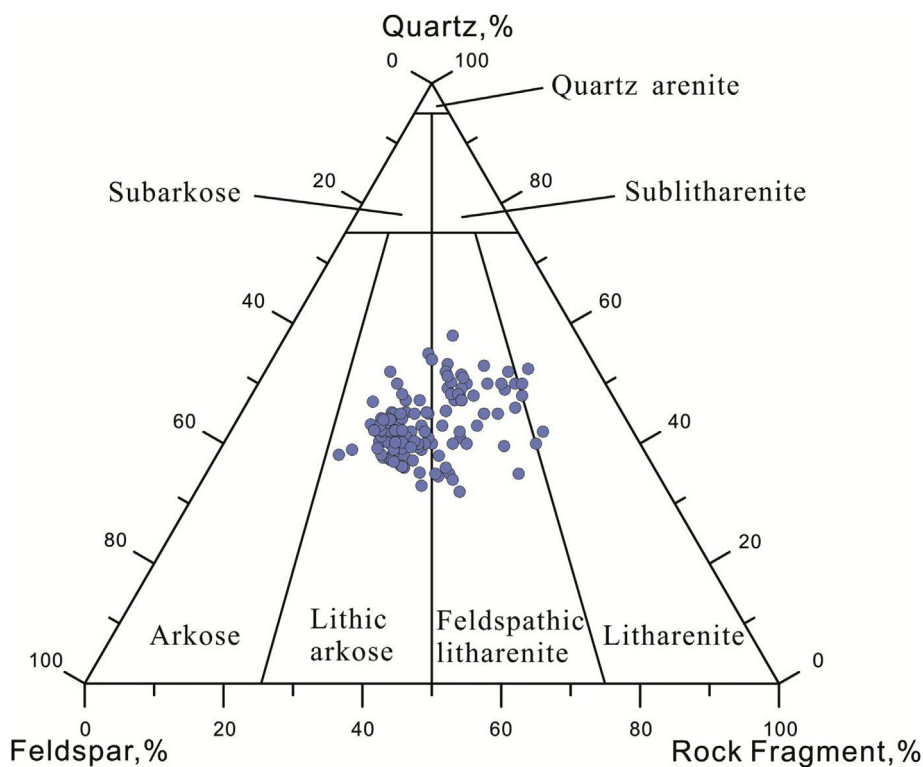


Fig. 6. Ternary diagram of rock composition of the K_1q_4 sandstones using Folk's (1974) classification.

(Table 1).

Dawsonite ($NaAlCO_3(OH)_2$), a carbonate mineral containing water, sodium and aluminium, has a relatively high content (1%–10%; av.6%) in the dawsonite-bearing sandstones. Dawsonite mainly occurs as radial, cluster or hair aggregates filling intergranular pores or replacing detrital grains (Fig. 7E, F, G and H), and sometimes occurs in feldspar dissolution pores (Fig. 7I). Dawsonit is relatively more abundant in the LST distributary channel sandstones than in TST distributary channel sandstones (no dawsonite-bearing samples in HST sandstones; Table 1).

5.2.3. Clay minerals

According to the XRD data and SEM analysis, the authigenic clay minerals in K_1q_4 sandstones mainly consist of kaolinite, illite, mixed-layer illite-smectite (I/S) and chlorite, and the content ranges from 4.1% to 33.7% of the total rock volume with an average of 13.6%. The content of authigenic clay minerals varies with depositional facies and system tracts, the LST have the lower clay minerals content than the TST and HST sandstones (av.10.9%, 16.0% and 17.2% in the LST, TST, and HST sandstones, respectively), while the clay minerals are relatively less abundant in (underwater) distributary channel sandstones compared with crevasse splay and sheet sand sandstones within LST, TST and HST respectively (Table 1).

Kaolinite (0%–8.1, av.0.8%) is less common in the K_1q_4 sandstones, and is relatively more common in the (underwater) distributary channel sandstones compared with the crevasse splay and/or sheet sand sandstones within LST, TST and HST respectively (Table 1). Kaolinite mainly occurs as euhedral booklets and vermicular aggregates filling intergranular pores and is commonly accompanied with authigenic quartz, illite or mixed-layer I/S (Fig. 8A).

Mixed-layer I/S (0.3%–24.4%, av.8.6%) is the dominant clay mineral and is relatively more abundant in HST underwater distributary channel and sheet sand sandstones compared with the LST and TST sandstones (Table 1). Mixed-layer I/S mainly occurs as flaky aggregates that commonly exists as grain coating cement, or sometime occurs as primary intergranular pore-filling cement with the aggregates showing the honeycomb-like morphology (Fig. 8B).

Thin section and SEM observation reveals that illite (0.2%–12.1%, av.1.5%) mainly occurs as intergranular pore-filling and grain coating cement showing fibrous, flaky or honeycomb morphology, and sometimes bridges the pore-throat locally. Illite also occurs as a replacement of feldspar together with kaolinite in dissolution pores (Fig. 8C and D). Illite is common in all depositional facies and system tracts, while is also relatively more abundant in HST sandstones than that in the LST and TST sandstones (Table 1).

The authigenic chlorite (0%–8.5%, av.2.5%), comprising pseudo-hexagonal platelets which are perpendicular to the grain surfaces, occurs mainly as pore-lining rosette aggregates (Fig. 8E). Chlorite is relatively more abundant in (underwater) distributary channel sandstones compared with crevasse splay and sheet sand sandstones within LST, TST and HST respectively (Table 1), and is more abundant in LST distributary channel sandstones compared to the TST distributary channel sandstones followed by the HST (underwater) distributary channel sandstones.

5.2.4. Quartz cements

Authigenic quartz cements (ranging from 0.5% to 3%, with an average of 1.6%) mainly occur as two different types: quartz overgrowth and pore-filling outgrowth authigenic quartz (Fig. 7F). Quartz overgrowth is common and easy to distinguish from detrital grains in thin sections due to the existence of dust clay rims. Two generations of quartz overgrowth can be distinguished locally (Fig. 8G). The pore-filling outgrowth authigenic quartz is evident in SEM samples, and occurs as discrete, euhedral microquartz crystals approximately 10–50 μm in size, partly or completely filling intergranular pore space, and is found to be together with authigenic kaolinite and illite commonly (Fig. 8H and I). Quartz cements are common in all depositional facies and system tracts and the content varies little among them (Table 1).

5.2.5. Dissolution

Dissolution of unstable detrital grains (feldspar and volcanic fragments) is common in the K_1q_4 sandstones. The partial to complete dissolution of the feldspars is mostly along the cleavage, and is

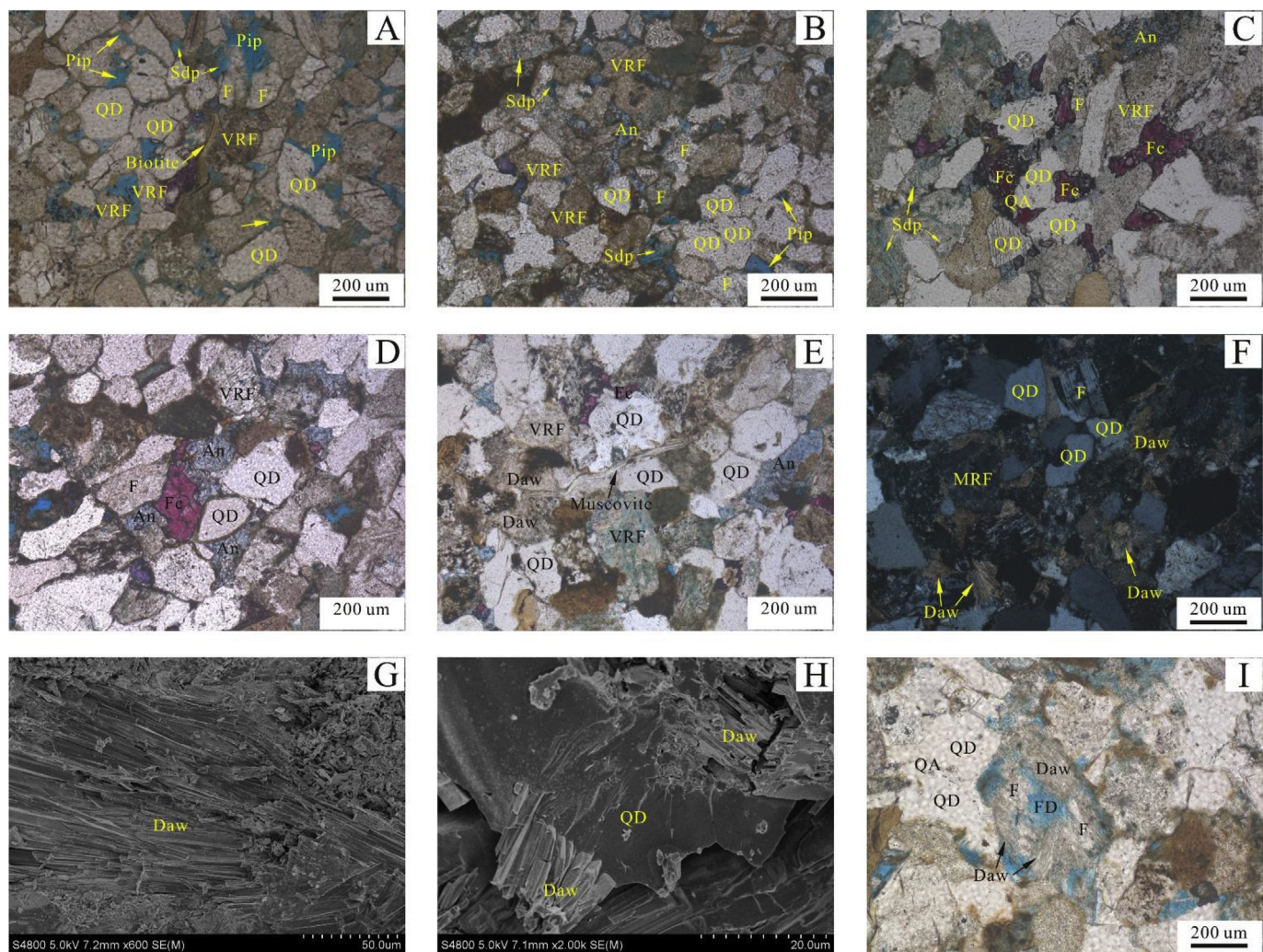


Fig. 7. The characteristics of compaction and carbonate cementation. (A) In PPL, deformation of biotite and volcanic rock fragments (well Mu249, 1238.2 m). (B) In PPL, lineal to concavo-convex grain contacts and deformation of volcanic rock fragments (well Qian48, 1206.7 m). (C) In PPL, ferrocalcite and ankerite filled the primary pores and secondary pores (well Gu27, 1214.9 m). (D) In PPL, ferrocalcite is replaced by ankerite (well Qian48, 1204.7 m). (E) In PPL, dawsonite filled the intergranular pores (well Gu27, 1216.4 m). (F) In PPL, dawsonite filled the intergranular pores and replaced the detrital grains (well Qian57, 1245.9 m). (G) SEM image showing the characteristics of dawsonite (well Gu27, 1206.7 m). (H) From SEM, dawsonite replaced the quartz (well Gu27, 1206.7 m). (I) In PPL, dawsonite filled the feldspar dissolution pores (well Gu27, 1198.3 m). XPL-cross-polarized light; PPL-plane-polarized light; QD-detrital quartz grains; QA-authigenic quartz; F-feldspar; VRF-volcanic rock fragments; MRF-metamorphic rock fragments; Daw-dawsonite; FD-feldspar dissolution; Pip-primary intergranular pores; Sdp-secondary dissolution pores.

commonly associated with kaolinite and microcrystalline authigenic quartz (Figs. 7I and 8I). The secondary dissolution porosity range from 0.1% to 4.0%, with an average of 1.1%. The secondary dissolution porosity varies among the different depositional facies and system tracts, the LST sandstones have the higher secondary dissolution porosity compared with the TST sandstones followed by the HST sandstones. Besides, the channel sandstones have relatively higher secondary dissolution porosity compared with crevasse splay and sheet sand sandstones within LST, TST and HST respectively (Table 1).

5.3. Reservoir quality of the K_1q_4 sandstones

The K_1q_4 sandstone reservoirs in the study area are of low permeability to tight reservoir. The helium porosity of the studied K_1q_4 sandstones ranges from 1.0% to 20.4% (mostly less than 14.0%) with an average of 11.32%, and horizontal permeability ranges from 0.01mD to 60.4mD (mostly less than 1mD) with an average of 0.884mD.

Thin section and SEM observation demonstrate that the porosity of the K_1q_4 reservoirs consists of primary intergranular pores, secondary

dissolution pores, and micro-pores. The primary intergranular pores (trace to 13%, av. 2.65%) have been shrunk by mechanical compaction and cementation. The primary intergranular pores are mainly triangle or polygonal in shape, and have relatively larger pore size compared to secondary dissolution pores (Fig. 7A). The secondary dissolution pores (trace to 4%, av. 0.73%), consisting mostly of partly to entirely dissolution of feldspar grains along the cleavage, is irregular in shape (Fig. 7A and B). The dissolution pores occurring along the edge of feldspar grains enlarges the adjacent primary intergranular pores or forms new intergranular pores (Fig. 7A). Pores existed in clay aggregates (such as mixed-layer I/S, illite, kaolinite, and chlorite) comprise the micropores (Fig. 8A-E). The content of micropores is estimated by the difference between helium porosity and thin section porosity (Dutton and Loucks, 2010), and ranges from tract to 15.7% with average of 9.01%.

The helium porosity of the LST sandstones (1555 samples) ranges from 1.6% to 19.7% (av. 11.37%), and the horizontal permeability ranges from 0.01mD to 60.4mD (av. 1.013mD). The TST sandstones (1958 samples) have the higher helium porosity than the HST and

Table 1

Modal composition of sandstone samples from the fourth member of Quantou formation in the study area. \: no sample.

Depositional facies and sequence stratigraphy	UWCH HST (n = 9)					SS HST (n = 5)					CH TST (n = 86)					CS TST (n = 13)					CH LST (n = 45)					CS HST (n = 11)				
	Min	Max	Mean	S.D	Min	Max	Mean	S.D	Min	Max	Mean	S.D	Min	Max	Mean	S.D	Min	Max	Mean	S.D	Min	Max	Mean	S.D	Min	Max	Mean	S.D		
Detrital component																														
Quartz	25.6	29.8	27.3	1.7	24.7	32.8	27.7	3.4	25.3	42.3	33.6	3.3	22.3	31.6	28.6	3.6	26.4	41.4	32.3	3.6	22.8	41.5	30.7	5.0						
Feldspars	22.0	26.3	24.5	1.3	11.0	22.8	18.6	5.1	16.9	26.5	20.0	4.9	19.6	23.8	22.3	1.7	19.8	32.4	23.3	5.5	12.3	27.8	22.4	5.5						
Volcanic fragments	14.6	17.8	15.3	1.2	14.8	22.2	18.9	3.4	12.6	31.4	19.1	3.8	14.0	26.6	18.3	4.8	12.8	29.4	19.4	5.0	13.6	26.0	18.2	4.2						
Sedimentary rock fragments	0.0	2.1	0.8	0.8	0.0	1.0	0.7	0.2	0.4	2.0	0.9	0.6	0.4	2.0	1.2	0.4	0.3	3.0	1.2	0.8	0.0	1.0	0.5	0.5						
Metamorphic fragments	0.4	3.4	2.3	1.2	0.2	1.9	1.1	0.6	0.5	11.4	1.9	1.4	0.2	1.5	0.9	0.5	0.3	2.8	1.6	0.7	0.5	2.8	1.3	0.7						
Mica	0.5	1.0	0.6	0.2	0.0	0.0	0.0	0.0	0.5	1.0	0.6	0.2	0.5	1.0	0.6	0.2	0.5	3.0	0.7	0.5	0.0	0.5	0.3	0.2						
Matrix	1.0	5.0	2.4	1.3	2.0	5.0	3.8	1.5	0.2	10.0	2.1	1.7	2.0	10.0	5.4	3.5	0.3	12.0	3.1	2.6	1.0	3.0	1.5	0.7						
Diagenetic alterations																														
Quartz overgrowth and outgrowth	1.0	2.0	1.6	0.4	1.0	3.0	1.8	0.9	1.0	3.0	1.5	0.4	1.0	3.0	1.6	0.7	0.5	3.0	1.7	0.6	0.5	3.0	1.8	0.8						
Ferrocalcite	0.0	13.0	4.7	4.8	0.1	10.3	3.8	3.2	0.0	14.0	1.5	2.8	0.8	12.0	3.1	3.4	0.0	18.0	1.6	2.9	0.0	3.0	1.4	1.2						
Ankerite	0.0	3.0	0.4	0.7	0.0	2.0	1.1	0.2	0.0	23.0	3.5	5.2	0.0	2.2	0.5	0.9	0.0	8.0	1.4	1.9	0.0	3.1	1.2	1.5						
Dawsonite	\	\	\	\	\	\	\	\	0.0	9.0	1.9	3.0	0.0	0.0	0.0	0.0	0.0	10.0	1.6	3.0	0.0	7.0	1.5	2.6						
I/S	1.9	26.1	12.2	5.4	7.2	24.0	17.2	7.7	4.1	23.4	9.2	5.7	0.3	25.6	13.9	7.7	1.8	23.4	6.2	4.3	4.3	20.6	11.1	6.4						
Illite	0.7	3.8	1.9	1.0	1.8	5.3	3.7	1.8	0.5	6.9	1.7	1.6	0.6	12.1	3.6	3.6	0.2	5.2	1.1	1.0	0.5	5.2	2.2	1.9						
Kaolinite	0.0	4.5	1.2	1.4	0.3	1.1	0.6	1.0	0.0	8.1	1.3	1.7	0.3	2.8	1.1	0.9	0.0	4.9	0.4	0.8	0.0	0.0	0.0	0.0						
Chrolite	0.0	3.8	0.8	1.1	0.0	0.2	0.1	0.0	0.2	6.2	2.5	1.8	0.1	6.3	2.0	2.7	0.0	8.5	3.4	1.8	0.0	5.9	2.4	1.9						
Point counting Porosity																														
Intergranular porosity	0.1	5.0	1.8	1.4	0.2	2.5	1.0	1.0	0.1	12.0	2.7	2.9	0.1	4.5	1.6	1.2	0.1	10.0	2.9	2.3	0.3	4.0	1.8	1.3						
Secondary porosity	0.2	1.5	0.7	0.5	0.1	0.5	0.2	0.2	0.1	3.0	0.7	0.7	0.1	1.5	0.6	0.5	0.1	3.5	1.2	0.7	0.1	1.0	0.7	0.4						

LST sandstones (Table 2), ranging from 2.8% to 20.4% (av. 11.51%), and have moderate horizontal permeability ranging from 0.01mD to 40.8mD (av. 0.683mD). The helium porosity and horizontal permeability of the HST sandstones (586 samples) ranges from 1.3% to 19.1% (av. 10.2%) and 0.01mD to 25.2mD (av. 0.354mD), respectively (Table 2). Thin section observation revealed that the intergranular porosity of the HST sandstones (14 samples), TST (99 samples) and LST (56 samples) sandstones range from 0.1% to 6% (av. 2.1%), 0.1%–13% (av. 2.6%) and 0.1%–10% (av. 2.6%), respectively (Table 1). The secondary dissolution porosities of the HST, TST and LST sandstones vary from 0.1% to 2% (av. 0.51%), 0.1%–4% (av. 0.74%), and 0.1%–3.5% (av. 0.68%), respectively.

The sandstones from the distributary channels of the delta plain in the lowstand system tracts (1347 samples) have an average helium porosity of 12.6% and an average horizontal permeability of 1.152mD, while the average helium porosity and horizontal permeability of the crevasse splay sandstones (208 samples) is 6.8% and 0.249mD, respectively. The average helium porosity and horizontal permeability of the distributary channel sandstones deposited in a delta plain (1758 samples) of the transgressive systems tracts are 12.7% and 0.728mD, respectively; while those of the crevasse splay sandstones (173 samples) are 6.6% and 0.287mD, respectively. The underwater distributary channel sandstones (509 samples) have higher average helium porosity (10.5%) and horizontal permeability (0.416mD) than those of the sheet sand (6.1% and 0.176mD, respectively, 77 samples) within the highstand system tracts.

5.4. Fluid inclusions

To determine the precipitation temperatures of the authigenic cements, the aqueous inclusions occurring in the authigenic quartz cements and the carbonate cements were selected through thin section observation. The selected fluid inclusions have a diameter ranging from

about 2.6 to 10.8 μm , and most of them are two phases at room temperatures, consisting of an aqueous phase and a gas bubble (Fig. 9).

The homogenization temperatures (T_h) of 25 aqueous inclusions present in the quartz overgrowths and 2 aqueous inclusions present in the pore-filling authigenic quartz in this study were measured (Table 3), with the temperatures ranging from 65.8 °C to 118.2 °C. The homogenization temperatures of the aqueous inclusions in the dawsonite range from 92.8 °C to 97.3 °C, and those of the ferrocalcite or ankerite range from 90.6 °C to 115.9 °C (Table 3). The results suggest that the carbonate cements formed subsequent to the precipitation of the authigenic quartz cements, which is consistent with thin section observation (Fig. 7C and D).

6. Discussion

6.1. Source of carbonate cements

The sources of carbonate cements including external, internal or mixed sources (Dutton, 2008), thin section observation reveals that there is no occurrence of detrital carbonate grains or bioclasts in the K₁q₄ sandstones, suggesting the internal source may be invalid for the carbonate cements. The adjacent mudstones and source rocks can provide the needed ions for the precipitation of carbonate cements (Dutton and Loucks, 2010; Yuan et al., 2015; Xi et al., 2015a,b). The relatively negative $\delta^{13}\text{C}$ values (−10.1‰ ~ −2.3‰) of carboanate cements in the K₁q₄ sandstone (Table 4) suggests that the organic matter decarboxylation from the adjacent mudstones and the overlying source rocks provide an important carbon source for the carbonate cements (Irwin et al., 1977; Curtis, 1978). According to the different combinations of carbonate cements, the sandstone samples are divided into two types in this section, dawsonite-bearing samples (dawsonite and ankerite) and samples without dawsonite (ankerite and ferrocalcite), to discuss the carbon sources of carbonate cements.

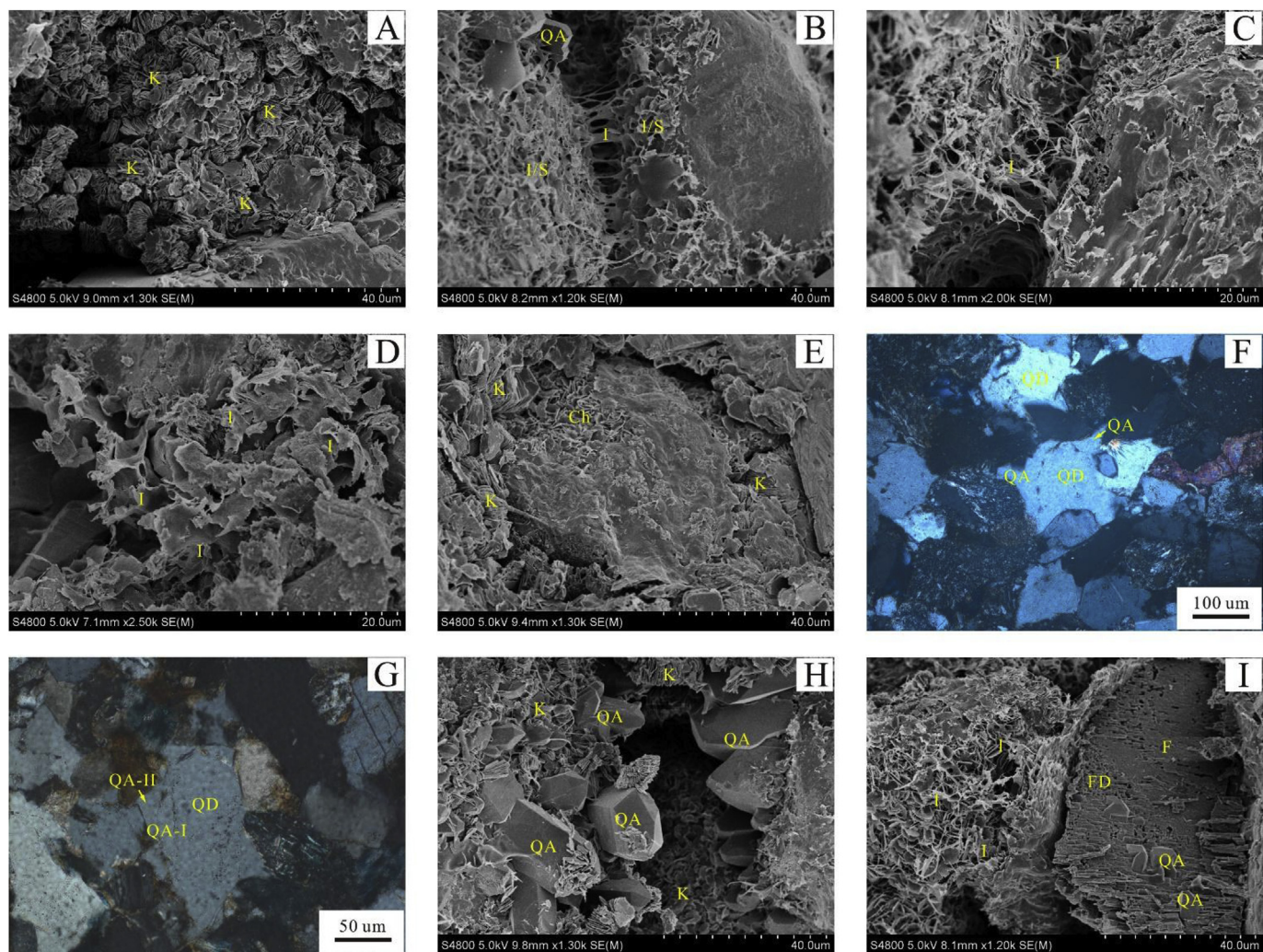


Fig. 8. The characteristics of clay minerals, quartz cementation and feldspar dissolution. (A) From SEM, kaolinite filled the intergranular pores (well Qian48, 1185.9 m). (B) SEM image showing illite and mixed-layer illite/smectite (well Mu249, 1240.6 m). (C) SEM image showing fibrous illite (well Rang37, 1596.9 m). (D) SEM image of the flaky illite (well Qian48, 1204.7 m). (E) SEM image showing the chlorite and kaolinite (well Qian41, 877.8 m). (F) In XPL, the quartz overgrowth and the pore-filling quartz (well Rang36, 1727.9 m). (G) In XPL, two generations of quartz overgrowth (well Gu27, 1198.3 m). (H) From SEM, the euhedral quartz crystals coexisting with kaolinite (well Qian61, 1272.9 m). (I) SEM image of the dissolution pores along the feldspar cleavage (well Rang37, 1596.9 m). XPL-cross-polarized light; PPL-plane-polarized light; QD-detrital quartz grains; QA-authigenic quartz; F-feldspar; VRF-volcanic rock fragments; MRF-metamorphic rock fragments; Daw-dawsonite; FD-feldspar dissolution; K-kaolinite; I-illite; Ch-chlorite; Mp-micropores.

The cross plots of the distance from the adjacent sandstone-mudstone contact surface versus the content of ferrocalcite, ankerite and dawsonite respectively both in dawsonite-bearing sandstone samples and sandstone samples without dawsonite show that the ferrocalcite and ankerite content decreases with the increasing distance (Fig. 10), but dawsonite content show weak correlation with the distance. Besides, for the sandstone samples without dawsonite, the $\delta^{13}\text{C}$ values of the carbonate cements increases with increasing distance from the overlying source rocks (Fig. 11). Both of them mentioned above provide evidence for ferrocalcite and ankerite in the sandstones affected by the adjacent mudstones and overlying source rocks, while the adjacent mudstones and overlying source rocks carbon source may not be a main carbon source for dawsonite. Dawsonite is the indicator mineral for CO_2 charging, and the $\delta^{13}\text{C}$ values of the dawsonite in the study area (Table 4) range from $-3.8\text{\textperthousand}$ to $-2.6\text{\textperthousand}$, and is also similar to the $\delta^{13}\text{C}$ values of the dawsonite (Liu et al., 2011; Yu et al., 2014; Qu et al., 2016) in other areas of the southern Songliao basin, which suggests the dawsonite in the southern Songliao basin have the similar carbon source. The previous studies revealed that the carbon source of dawsonite in the southern Songliao basin is provided by inorganic CO_2

originated from mantle-derived magma (Gao et al., 2007; Liu et al., 2011; Yu et al., 2014; Qu et al., 2016), which indicates that the carbon source of dawsonite in the study area is mainly provided by the inorganic CO_2 originated from mantle-derived magma.

The precipitation temperatures of ankerite, ferrocalcite and dawsonite were calculated with assuming $\delta^{18}\text{O}_{\text{SMOW}}$ values of $-7.0\text{\textperthousand}$ (Xi et al., 2015b). The oxygen isotope fractionation factor for dolomite-water of Matthews and Katz (1977) was used to calculate temperatures of ankerite and dawsonite, and that for calcite-water of Friedman and O'Neil (1977) was used for calculation of ferrocalcite temperatures. The calculated temperatures of ankerite, ferrocalcite and dawsonite are close, ranging from 93.68°C to 127.74°C , 83.22°C - 124.39°C , and 88.16°C - 99.46°C , respectively, suggesting that dawsonite formed slightly latter than ferrocalcite and earlier than ankerite, which is similar to the homogenization temperature measured from carbonate cements (Table 2) and consistent with thin section observation (Fig. 7D and E). Meanwhile, the $\delta^{13}\text{C}$ values of carboanate cements in the dawsonite-bearing sandstone samples range from $-5.7\text{\textperthousand}$ to $-2.6\text{\textperthousand}$, and is similar to the $\delta^{13}\text{C}$ values ($-10.1\text{\textperthousand}$ ~ $-2.3\text{\textperthousand}$) of carbonate cements in the sandstone samples without dawsonite, which suggests

Table 2

The ranges of helium porosities and permeabilities of the LST, TST and HST sandstones, and the average helium porosities, permeabilities, sorting coefficients and mean grain diameters of sandstones from different depositional facies within the LST, TST and HST.

System tracts	Helium porosity(%)			Helium permeability(mD)		
	Min	Max	Ave	Min	Max	Ave
HST	1.3	19.1	10.17	0.01	25.2	0.354
TST	2.8	20.4	11.51	0.01	40.8	0.683
LST	1.6	19.7	11.37	0.01	60.4	1.013

System tracts	Depositional facies	Average helium porosity (%)	Average helium permeability (mD)	Sorting coefficient	Mean grain diameter
HST	Underwater distributary channel	10.5	0.416	2.23	0.040
TST	Sheet sand	6.1	0.176	2.44	0.038
	Distributary channel	12.7	0.974	2.31	0.056
LST	Crevasse splay	8.6	0.249	3.39	0.022
	Distributary channel	12.6	1.152	2.23	0.075
	Crevasse splay	8.8	0.287	3.62	0.031

the carbonate cements in the dawsonite-bearing sandstones is also affected by the adjacent mudstones and the overlying source rocks. Therefore, the carbon sources of carbonate cements in the K₁q₄ sandstones are mixture sources of inorganic CO₂ originated from mantle-derived magma and organic CO₂ originated from decarbonylation of organic matter from the adjacent mudstones and the overlying source rocks. For the dawsonite-bearing sandstones, the mantle-derived magmatic CO₂ is the main carbon source for the carbonate cements; while for the sandstones without dawsonite, the carbon sources of carbonate cements is provided by mostly the adjacent mudstones and overlying

source rocks, and few organic CO₂ generated by hydrocarbon source rocks.

Ca²⁺, Mg²⁺ and Fe²⁺ are required to be present in the formation water to precipitate the ferrocalcite and ankerite, and Na⁺ and Al³⁺ are also needed for the precipitation of the dawsonite. The dissolution of volcanic rock fragments in the sandstones can provide Ca²⁺, Fe²⁺ and Mg²⁺ ions, and the conversions of clay mineral, such as smectite to illite occurred in the sandstones and the adjacent mudstones and source rocks, are also important sources for those ions (Boles and Franks, 1979; McHargue and Price, 1982; Yuan et al., 2015; Xi et al., 2015b). Na⁺ and Al³⁺ ions have many potential sources. The organic acid generated by mature hydrocarbon source rock, and inorganic CO₂ facilitated the dissolution of plagioclase which can provide Na⁺ and Al³⁺ ions, and the dissolution of potassium feldspar can be a source of Al³⁺ ions (Heritsch, 1975; Worden, 2006; Liu et al., 2011). Besides, the hydrothermal fluids containing abundant inorganic CO₂ can also provide some alkali metal ions. The formation of dawsonite needs an alkaline - weakly acidic fluid environment with high partial CO₂ pressure and temperature ranging from 25 °C to 100 °C, and high CO₂ partial pressure in the formation water is primary for the dawsonite precipitation (Qu et al., 2008, 2010), which can explain why not each sample contains dawsonite. It can be concluded that dawsonite and the coupled ankerite mainly precipitated in the sandstones on the main migration pathways or the accumulation zones of mantle-derived CO₂ which had high CO₂ partial pressure, while other sandstones with relatively small amounts of influx of mantle-derived CO₂ mainly precipitated ankerite and ferrocalcite.

6.2. Paragenetic sequence of diagenesis

Based on texture relationship, the relative sequence of the main diagenetic events of the K₁q₄ sandstones in the study area has been determined through thin section and SEM observation. Through the measurement of the fluid inclusions and the calculation of the oxygen isotope values, the formation temperatures of the quartz cements and carbonate cements can be obtained, which can help to provide a

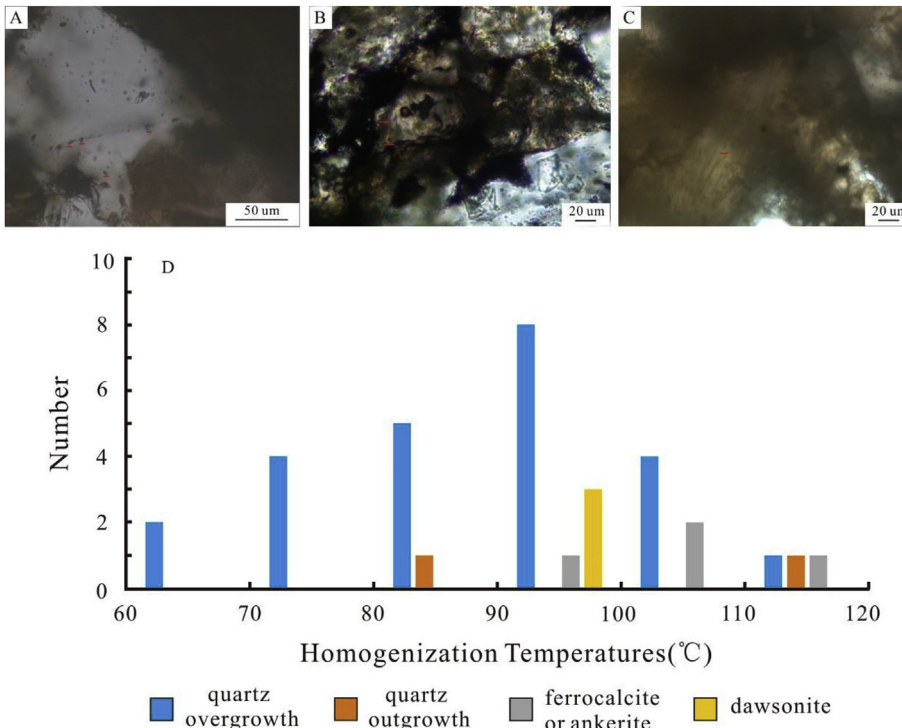


Fig. 9. (A–C) Photomicrographs of aqueous inclusions in quartz overgrowth and outgrowth, ferrocalcite or ankerite, and dawsonite respectively. (D) Histograms of homogenization temperatures (T_h) of fluid inclusions in K₁q₄ sandstones.

Table 3

Homogenization temperature data of fluid inclusions in authigenic quartz cements and carbonate cements of the K₁q₄ sandstones. T_h: homogenization temperature.

Well	Depth(m)	Hosted mineral	Th(°C)	Well	Depth(m)	Hosted mineral	Th(°C)
Gu27	1190.8	Quartz overgrowth	87.6	Qian57	1248.8	Quartz overgrowth	75.2
Gu27	1190.8	Quartz overgrowth	88.4	Qian57	1248.8	Quartz overgrowth	89.1
Gu27	1190.8	Quartz overgrowth	94.8	Qian57	1248.8	Fc or An	102.7
Gu27	1190.8	Quartz outgrowth	118.2	Qian57	1248.8	Fc or An	115.9
Gu27	1190.8	Dawsonit	94.2	Qian48	1213	Quartz overgrowth	98.2
Gu27	1190.8	Dawsonit	97.3	Qian48	1213	Quartz overgrowth	104.3
Gu27	1235.7	Quartz overgrowth	95.3	Qian48	1213	Quartz overgrowth	108.7
Gu27	1235.7	Quartz overgrowth	98.4	Qian101	906.1	Quartz overgrowth	92.1
Gu27	1235.7	Quartz overgrowth	106.7	Qian101	906.1	Quartz overgrowth	101
Gu27	1235.7	Dawsonit	92.8	Qian101	906.1	Quartz overgrowth	112.3
Mu249	1238.2	Quartz overgrowth	78.3	Rang36	1658.9	Quartz overgrowth	85.4
Mu249	1238.2	Quartz overgrowth	92.4	Rang36	1658.9	Quartz overgrowth	89.8
Mu249	1238.2	Quartz overgrowth	96.8	Rang36	1658.9	Quartz overgrowth	92.7
Qian41	877.8	Quartz overgrowth	65.8	Rang37	1595.9	Quartz overgrowth	79.5
Qian41	877.8	Quartz overgrowth	67.3	Rang37	1595.9	Quartz overgrowth	92.4
Qian41	877.8	Quartz overgrowth	72.5	Rang37	1595.9	Fc or An	90.6
Qian41	877.8	Quartz outgrowth	87.3	Rang37	1595.9	Fc or An	104.6

Table 4

Mineralogical and isotopic composition of carbonate cements, and calculated formation temperature of cements in the K₁q₄ sandstones in the study area. Fc-ferrocalcite, An-ankerite, Daw-dawsonite.

Well	Depth(m)	Carbonate minerals	$\delta^{13}\text{C}_{\text{V}-\text{PDB}}(\text{\textperthousand})$	$\delta^{18}\text{O}_{\text{V}-\text{PDB}}(\text{\textperthousand})$	Temp.(°C) $\delta^{18}\text{O}_{\text{SMOW}} = -7\text{\textperthousand}$
Rang36	1658.88	Fc	-4.2	-22.2	121.05
Rang36	1712.38	Fc	-10.1	-22.5	124.40
Qian61	1286.65	Fc	-2.3	-18.3	83.22
Qian61	1291.6	An	-5.8	-19.3	106.41
Rang27	1570.79	An	-6.5	-20.7	119.58
Rang27	1589.4	An	-7.7	-21	122.58
Rang27	1591.43	An	-7.9	-20.9	121.57
Rang27	1598.72	An	-7.3	-20.9	122.58
Rang37	1595.88	An	-7.4	-21.4	127.74
Qian48	1179.5	An	-10.5	-16.8	85.12
Qian48	1206.3	An	-4.5	-18.6	100.31
Qian48	1213	An	-5.5	-14.9	70.97
Qian57	1245.88	20%Daw + 80%An	-2.6	-17.9	93.68
Qian57	1248.83	20%Daw + 80%An	-4	-17.9	93.68
Qian57	1262.98	10%Daw + 90%An	-5.7	-20.5	117.61
Gu27	1233.1	90%Daw + 10%An	-2.8	-17.1	88.16
Gu27	1190.75	80%Daw + 20%An	-2.6	-17.9	93.68
Gu27	1215	80%Daw + 20%An	-3.8	-18.5	99.46

Note: The equations used for fractionation between carbonates and water are: $1000\ln\alpha_{\text{calcite}/\text{ferrocalcite}-\text{water}} = 2.78 \times 10^6/T^2 - 2.89$ (Friedman and O'Neil, 1977) and $1000\ln\alpha_{\text{dolomite}/\text{ankerite}/\text{dawsonite}-\text{water}} = 3.06 \times 10^6/T^2 - 3.24$ (Matthews and Katz, 1977).

relatively more accurate timing of the diagenetic process. With the restraint of the formation temperatures of the authigenic cements and the burial-thermal history of the study area (Zou et al., 2007), the paragenetic sequence of diagenesis of the K₁q₄ sandstones in the study area is summarized in Fig. 12.

The main eodiagenetic events, including compaction, occur at depths of less than 1200 m with R_o values small than 0.5%. During the early mesogenetic stage, the R_o values ranges from 0.5% to 1.3%, and the burial depth exceeds 1200 m. The compaction proceeds, and the organic matter in the K₂qn₁ is mature and began to generate hydrocarbon by the end of Nengjiang age (85Ma) (Zou et al., 2007), the feldspars and volcanic rock fragments is dissolved by the organic acid generated by the hydrocarbon source rock, while the dissolution of potassium feldspar provide the potassium for the smectite to illite reaction which is also an important silicate source for the formation of authigenic quartz cements (Xi et al., 2015a). Accompanied by the exhaustion of the organic acid and the increasing concentration of alkali metal ions, the pore fluid turned to alkaline, and the late carbonate cements (ferrocalcite and ankerite) and dawsonite began to precipitate.

The precipitation of dawsonite mainly occurred in sandstones with high CO₂ partial pressure due to the charging of mantle-derived CO₂, and the dawsonite-bearing sandstones mainly distributed in the vicinity of deep-rooted faults. The charging of the mantle-derived CO₂ occurred from the end of the late Cretaceous Mingshui period to the Paleogene, and is slightly latter than or approximately the same as the second phase of hydrocarbon charging (Liu et al., 2011; Qu et al., 2016).

6.3. Factors controlling the reservoir quality

6.3.1. Impact of depositional facies within sequence stratigraphic framework on the reservoir quality

Depositional facies within sequence stratigraphic framework exerts a significant control on the porosity and permeability of the K₁q₄ sandstones. The porosity of the LST distributary channel sandstones is similar to that of the TST distributary channel sandstones, while the LST distributary channel sandstones have higher permeability than that of the TST distributary channel sandstones, and the HST underwater distributary sandstones have lowest porosity and permeability. The rising base level caused the increasing accommodation space and the retrogradation of sedimentary facies zone, and resulted in a relatively higher-energy environment during the period of LST compared with the TST and the HST. Therefore, the LST distributary channel and crevasse splay sandstones have the larger mean grain size than that of the TST distributary channel and crevasse splay sandstones followed by the HST underwater distributary channel and sheet sand sandstones (Table 2). Besides, the LST distributary channel sandstones are more amalgamated than TST and HST (underwater) distributary channel sandstones due to the low accommodation space, which resulted in better sandstones lateral connectivity in LST distributary channel sandstones than TST and HST (underwater) distributary channel sandstones. Moreover, the three of them have the similar sorting coefficient. All of these resulted in the relatively more intergranular pore space in LST distributary channel sandstones after mechanical compaction than that in the TST distributary channel sandstones and HST underwater distributary channel sandstones, which facilitated the circulation of the acid fluids and mass transfer of elements and contributed to more secondary porosity in LST distributary channel sandstones (Table 2 and Fig. 13). Besides, the (underwater) distributary channel sandstones have better reservoir quality than the sandstones from the crevasse splays and sheet sands within LST, TST and HST respectively. The distributary channel sandstones and the underwater distributary channel sandstones deposited in the relatively higher-energy environment than the sandstones from the crevasse splays and sheet sands, and are characterized by the large median grain diameter and good sorting (Table 2). The cross plots of median grain diameter versus porosity and

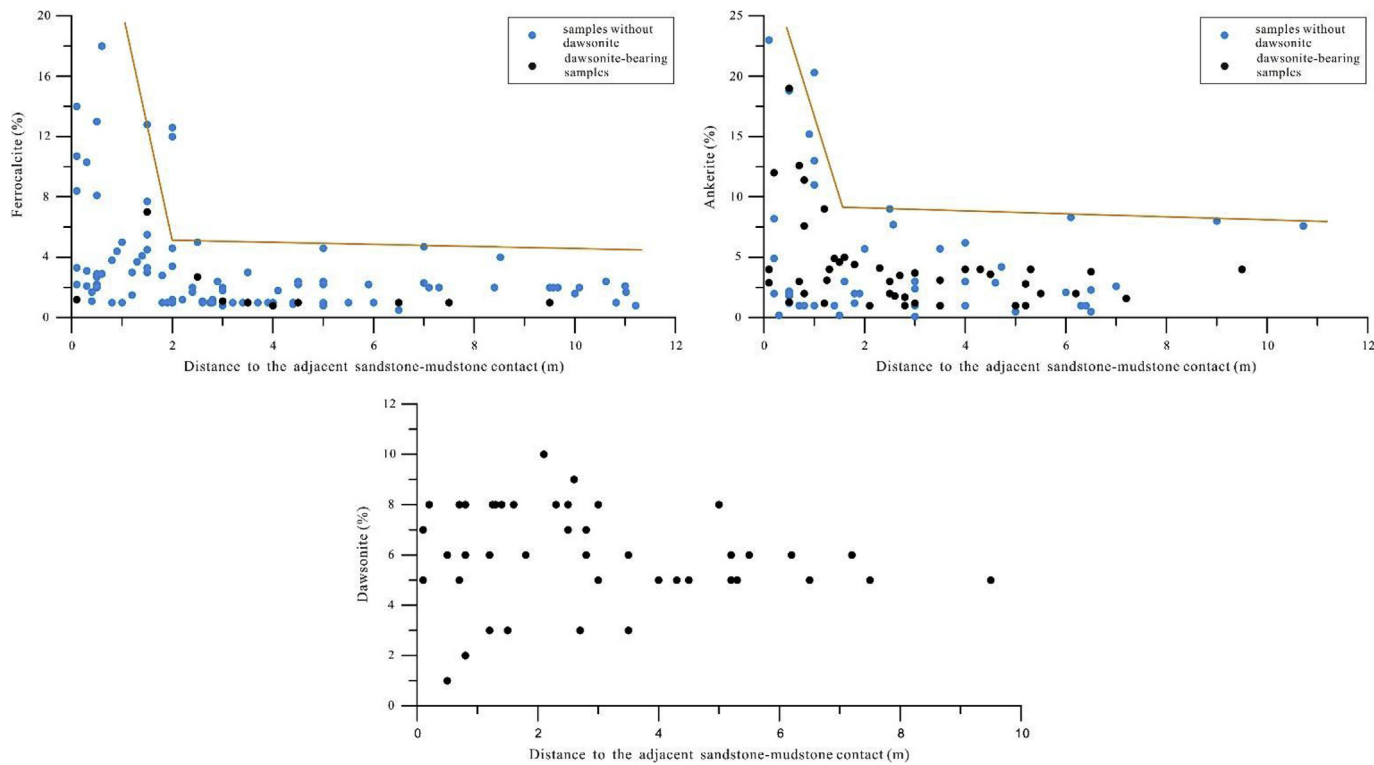


Fig. 10. The cross plots showing the relationship between the content of ferrocalcite, ankerite and dawsonite in different sandstone samples and the distance to the adjacent sandstone-mudstone contact.

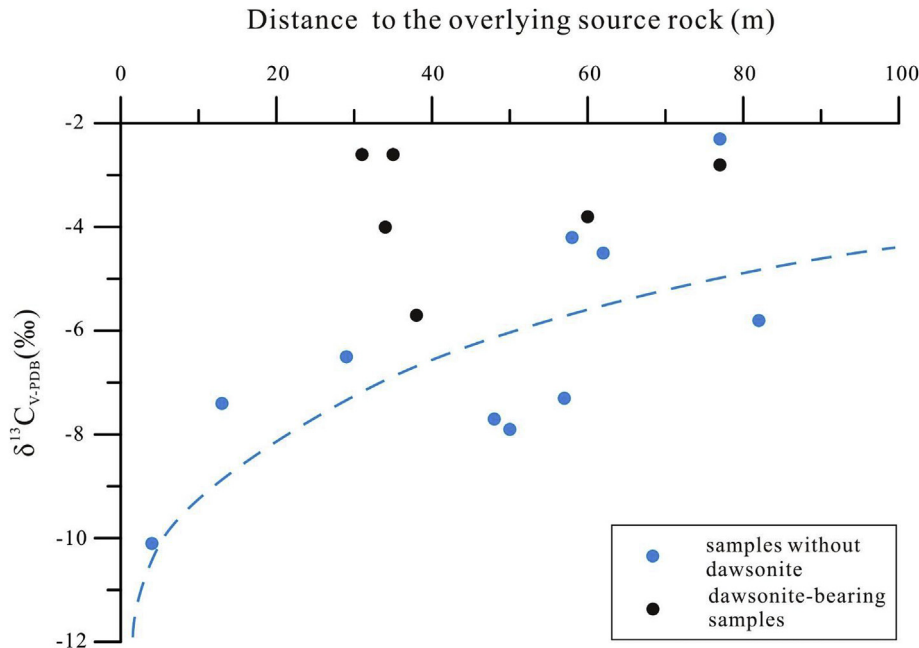


Fig. 11. The cross plot showing the relationship between the values of $\delta^{13}\text{C}$ of carbonate cements in different sandstone samples and the distance to the overlying source rock.

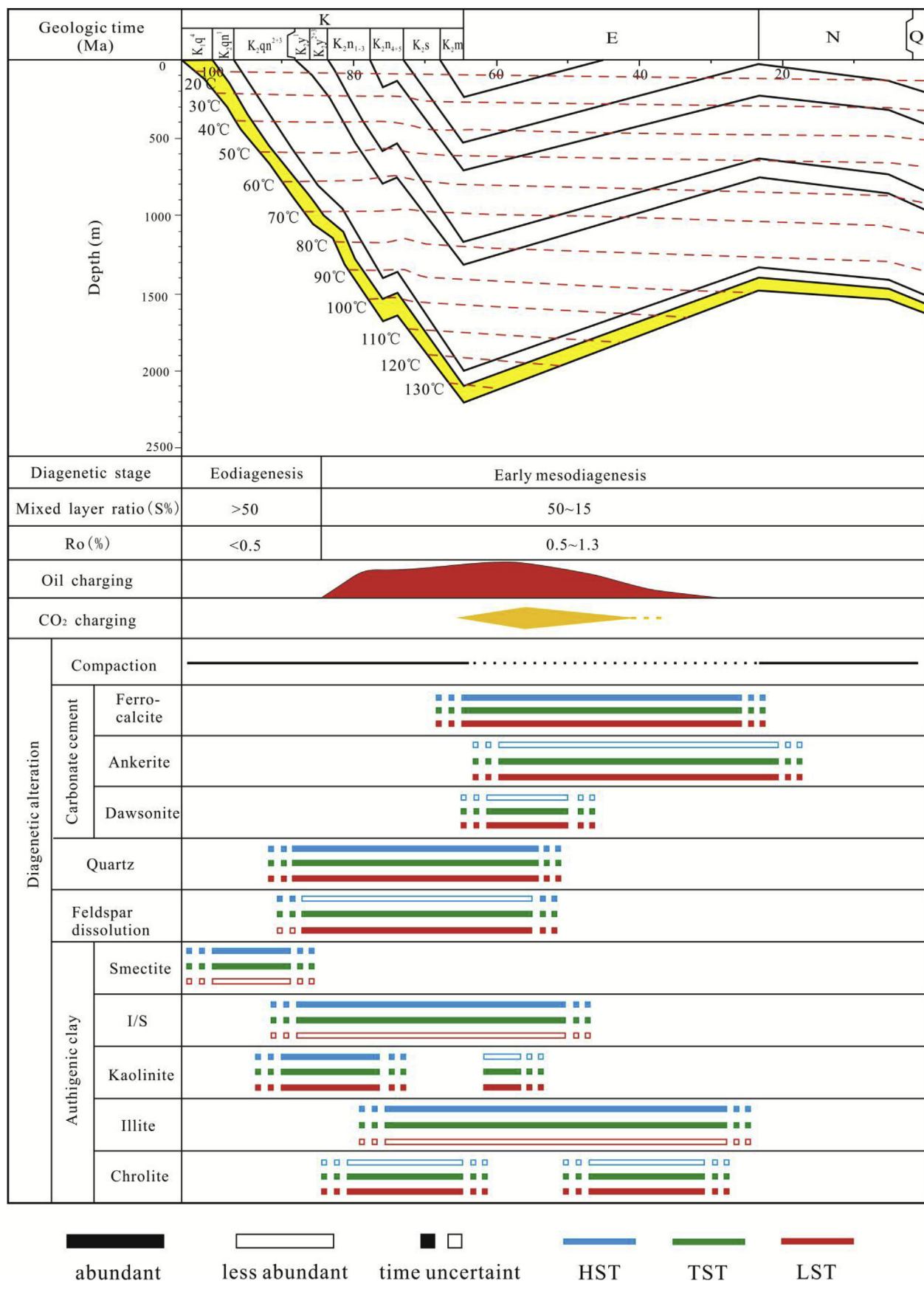
permeability respectively indicate that the reservoir quality of K₁q₄ sandstones increases with increasing grain size (Fig. 14).

6.3.2. Impact of diagenesis within the framework of sequence stratigraphy and depositional facies on the reservoir quality

6.3.2.1. Compaction. The K₁q₄ sandstones are shallow buried with burial depth less than 2000m, but compaction is intense (Fig. 7A and B). Petrologic analysis reveals that the K₁q₄ sandstones contain

relatively high ductile fragments content including volcanic fragments, micas and mudstones fragments, which exert an important control on the reservoir quality. The correlations between the ductile fragments content and porosity and permeability are negative (Fig. 15), suggesting that the sandstones with abundant mechanically unstable compositions generally suffer a quickly reduction in porosity and permeability during burial due to poor compression resistance.

The plot of intergranular volume versus cement volume, assuming

Fig. 12. Burial, thermal and diagenetic history of the K₁q₄ sandstone reservoirs.

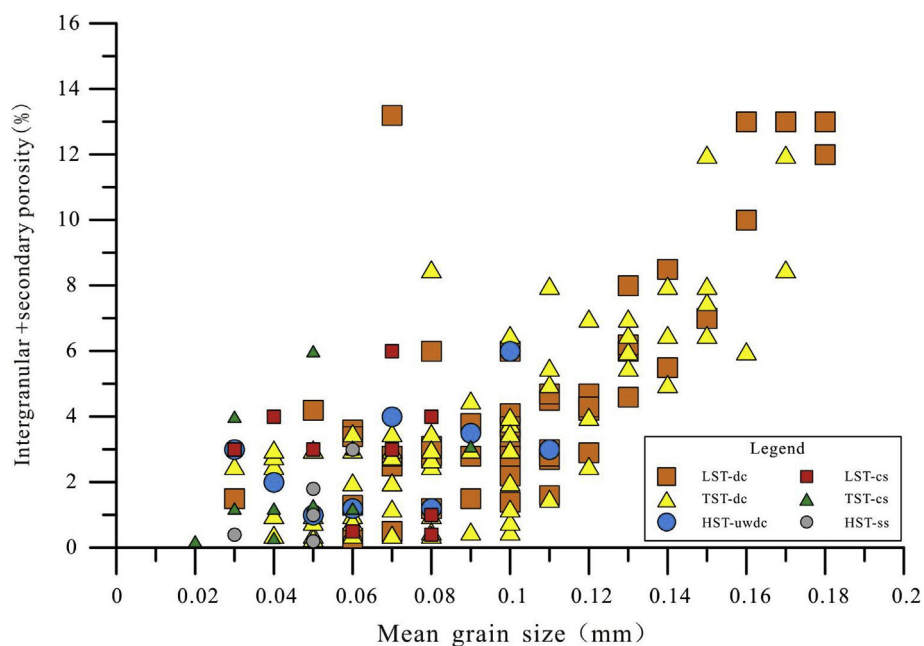


Fig. 13. Plot of intergranular + secondary porosity versus mean grain size based on thin section analysis for 212 sandstone samples. LST-lowstand system tract; TST-transgressive system tract; HST-highstand system tract; uwdc-underwater distributary channel; ss-sheet sand; dc-distributary channel; cs-crevasse splay.

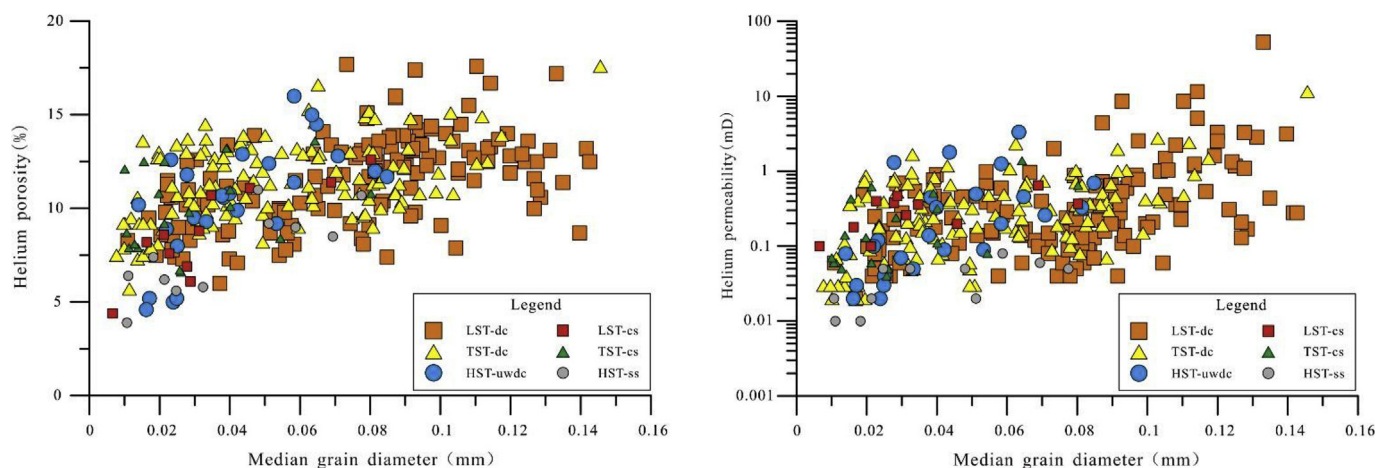


Fig. 14. The cross plots showing the relationship between median grain diameter and the helium porosity and permeability respectively. LST-lowstand system tract; TST-transgressive system tract; HST-highstand system tract; uwdc-underwater distributary channel; ss-sheet sand; dc-distributary channel; cs-crevasse splay.

the original porosity of K₁q₄ sandstones is 40% (Houseknecht, 1987), indicates that mechanical compaction is the major factor induced the original porosity loss compared to cementation (Fig. 16). The LST, TST and HST sandstones underwent a 75.2%, 74.7% and 77.4% reduction in original porosity by mechanical compaction (compaction rate) respectively, showing little difference among the different system tracts. However, the LST and TST distributary channel sandstones and HST underwater distributary channel sandstones underwent a 73.9%, 73.9% and 76.7% reduction in original porosity by mechanical compaction respectively, which is lower than that in sandstones from LST and TST crevasse splay and HST sheet sand respectively (81.4%, 79.6% and 78.6% respectively; Fig. 16).

The differences of compaction rate mentioned above among the different depositional facies within LST, TST and HST respectively depend on various factors, among which the ductile rock fragments contents and sorting coefficients of sandstones might be the key factors. However, the ductile rock fragments contents show little variations among the different system tracts and depositional facies, and the sorting coefficients of sandstones show variations with different

depositional facies within LST, TST and HST respectively (Table 2). The cross plot of the sorting coefficient versus compaction rate indicates that sandstones with higher sorting coefficient suffer more intensive grain stacking pattern with the small grains filling the intergranular pore space during burial, resulting in the relatively more compaction porosity loss, especially the sandstones with sorting coefficient greater than 2.5, mostly suffering compaction rate greater than 80% (Fig. 17), such as the sandstones from the crevasse splay and sheet sand (Table 2). The cross plots of porosity and permeability versus compaction rate indicate that the reservoir quality decreases with the increasing compaction rate when the compaction rate is greater than 80% approximately (Fig. 17). For the sandstones with compaction rate less than 80%, the correlation between the porosity reduction in original porosity by mechanical compaction and the reservoir quality is positive, suggesting that the low reservoir quality of sandstones is mainly caused by cementation in this case.

6.3.2.2. Cementation. Cementation is another significant factor that caused the reduction of porosity and permeability in the K₁q₄

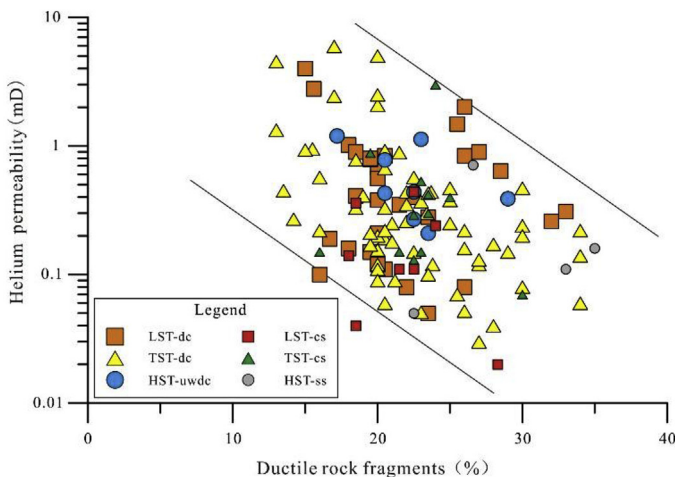
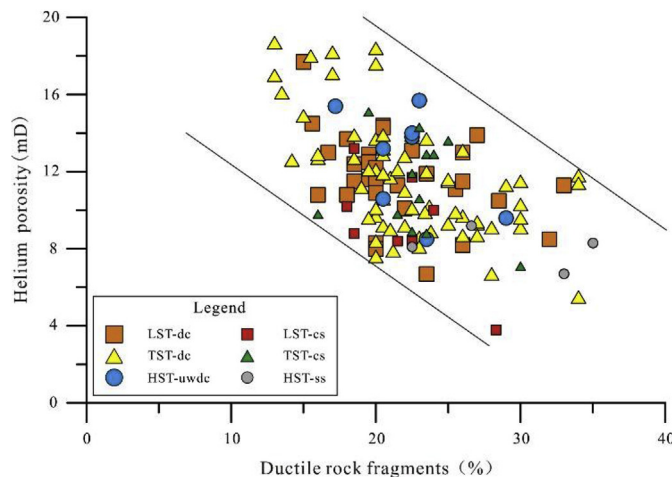


Fig. 15. Cross plots showing the relationship between the content of ductile rock fragments and helium porosity and permeability. LST-lowstand system tract; TST-transgressive system tract; HST-highstand system tract; uwdc-underwater distributary channel; ss-sheet sand; dc-distributary channel; cs-crevasse splay.

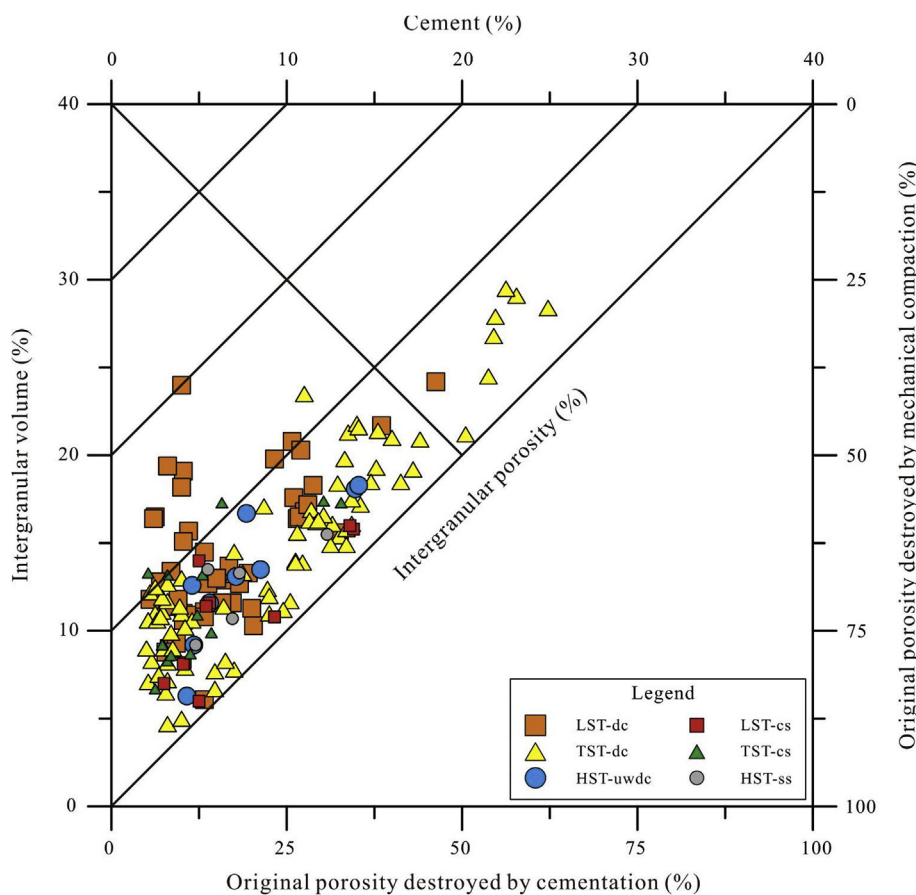


Fig. 16. Plot of cement volume versus intergranular volume in K_1q_4 sandstones showing the effects of compaction and cementation on porosity reduction (modified from Houseknecht, 1987 and Lundegard, 1992). LST-lowstand system tract; TST-transgressive system tract; HST-highstand system tract; uwdc-underwater distributary channel; ss-sheet sand; dc-distributary channel; cs-crevasse splay.

sandstones. The main cement types recognized in this study are quartz, carbonate cements and authigenic clay minerals. The cross plot of the cement volume versus intergranular volume of the K_1q_4 sandstone samples in the study area shows that the amount of porosity loss by cementation in the LST, TST and HST (underwater) distributary channel sandstones are 18%, 22.2% and 21.4%, respectively; while that in the sandstones from the LST and TST crevasse splay and HST sheet sand are 10.2%, 11.4% and 18.2%, respectively (Fig. 16).

The quartz cements were common in the K_1q_4 sandstones, and the content show little difference among the different system tracts and depositional facies (Table 1). The fluid inclusion results suggest that

there are two phase quartz overgrowth and the formation of quartz cements was a quasi-continuous process. The silica source of quartz cements were mainly internal sources and there are three primary silica source of quartz cements in the K_1q_4 sandstones: (1) smectite-to-illite reaction is the main silica source; (2) pressure dissolution can provide amounts of silica source; (3) the K-feldspar and kaolinite to illite reaction provide a few of silica source (Xi et al., 2015a,b). Variation in porosity reduction by quartz cement show little difference among the LST, TST and HST sandstones, with an average of 1.8%, 1.5% and 1.7% respectively.

Variations in the porosity and permeability with the carbonate

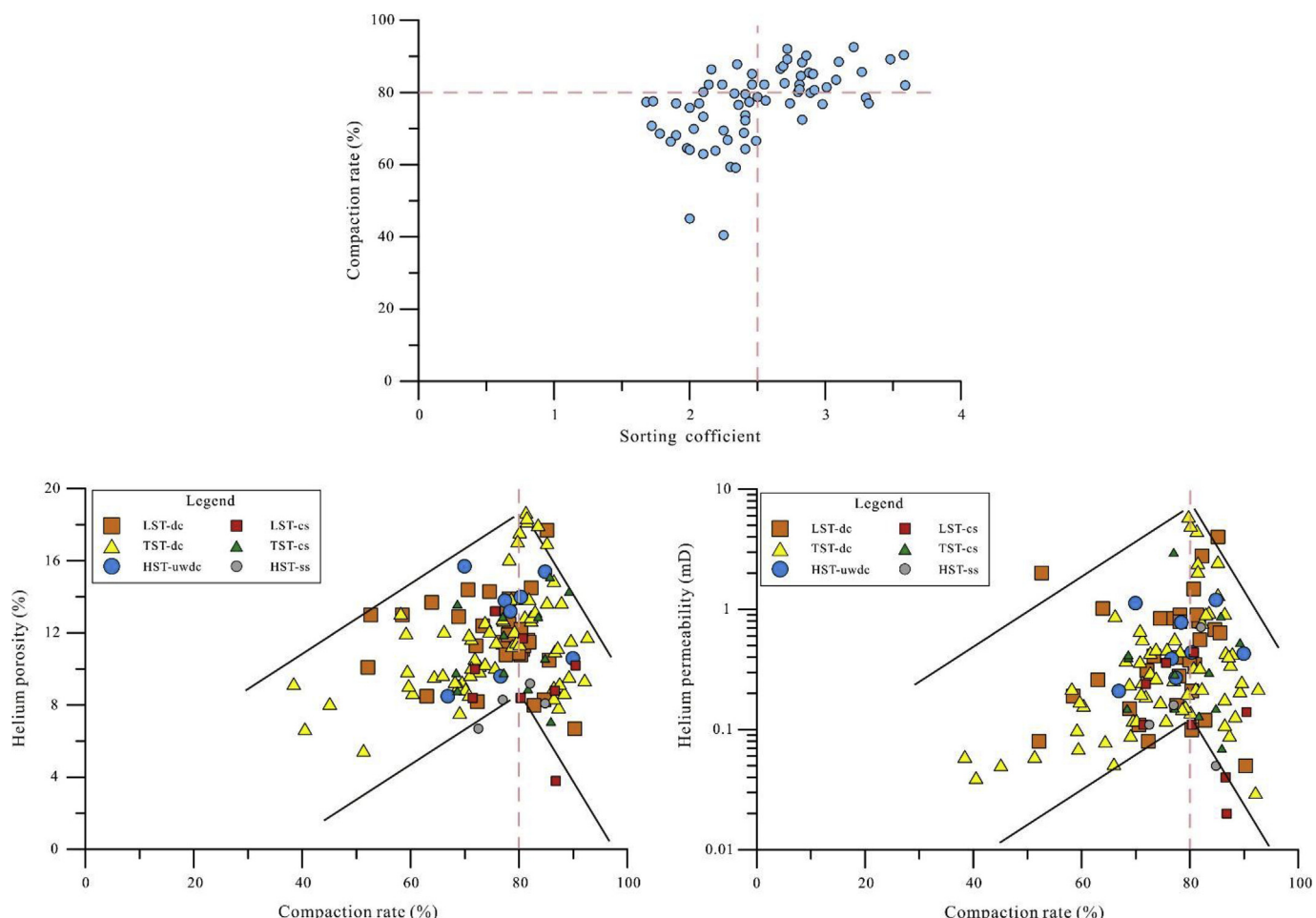


Fig. 17. Cross plots showing relationship between the sorting coefficient and compaction rate (upper), and the relationship between the compaction rate and helium porosity and permeability (lower). LST-lowstand system tract; TST-transgressive system tract; HST-highstand system tract; uwdc-underwater distributary channel; ss-sheet sand; dc-distributary channel; cs-crevasse splay.

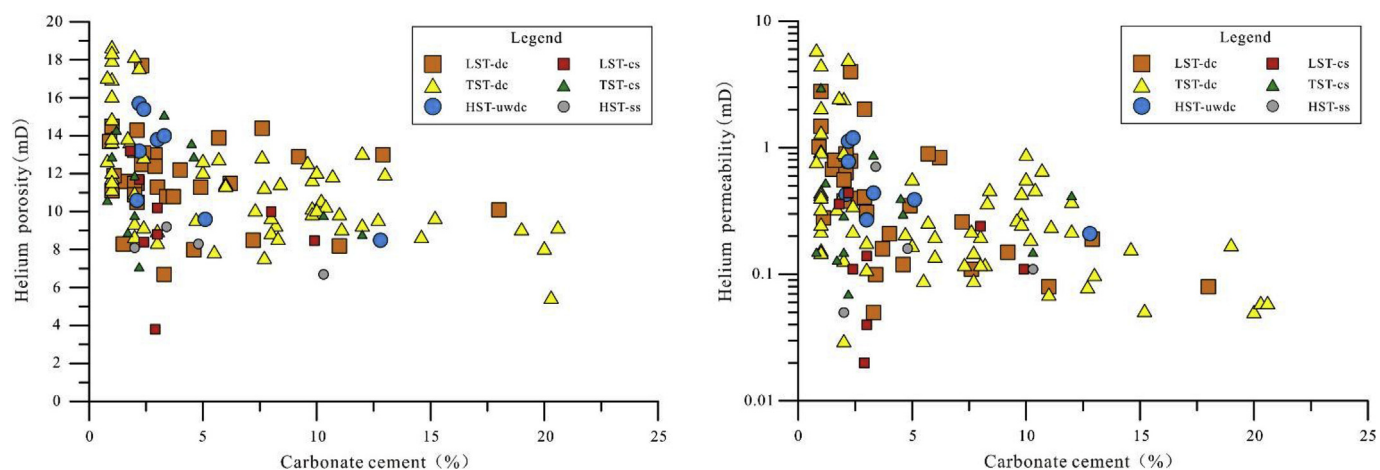


Fig. 18. Cross plots showing relationship between the carbonate cement content and helium porosity and permeability. LST-lowstand system tract; TST-transgressive system tract; HST-highstand system tract; uwdc-underwater distributary channel; ss-sheet sand; dc-distributary channel; cs-crevasse splay.

cements reveals that sandstones with abundant carbonate cements tend to have low reservoir quality, which suggests that carbonate cementation is a significant factor controlling the reservoir quality of the K₁q₄ sandstone reservoirs in the study area (Fig. 18). However, carbonate cement content varies substantially with different depositional facies and system tracts (Table 1). The HST and TST sandstones have relatively more abundant carbonate cement (av. 5.0% and 6.4%,

respectively) compared with the LST sandstones (av. 4.4%). The TST and HST sandstones are closer to the overlying source rocks, and the interbedded mudstones are better developed during the periods of TST and HST due to the increasing accommodation space, which can provide relatively more sufficient ions for carbonate cementation, compared with the LST sandstones. Moreover, the occurrence of the convection of the organic acid fluids and hydrotherm fluids containing

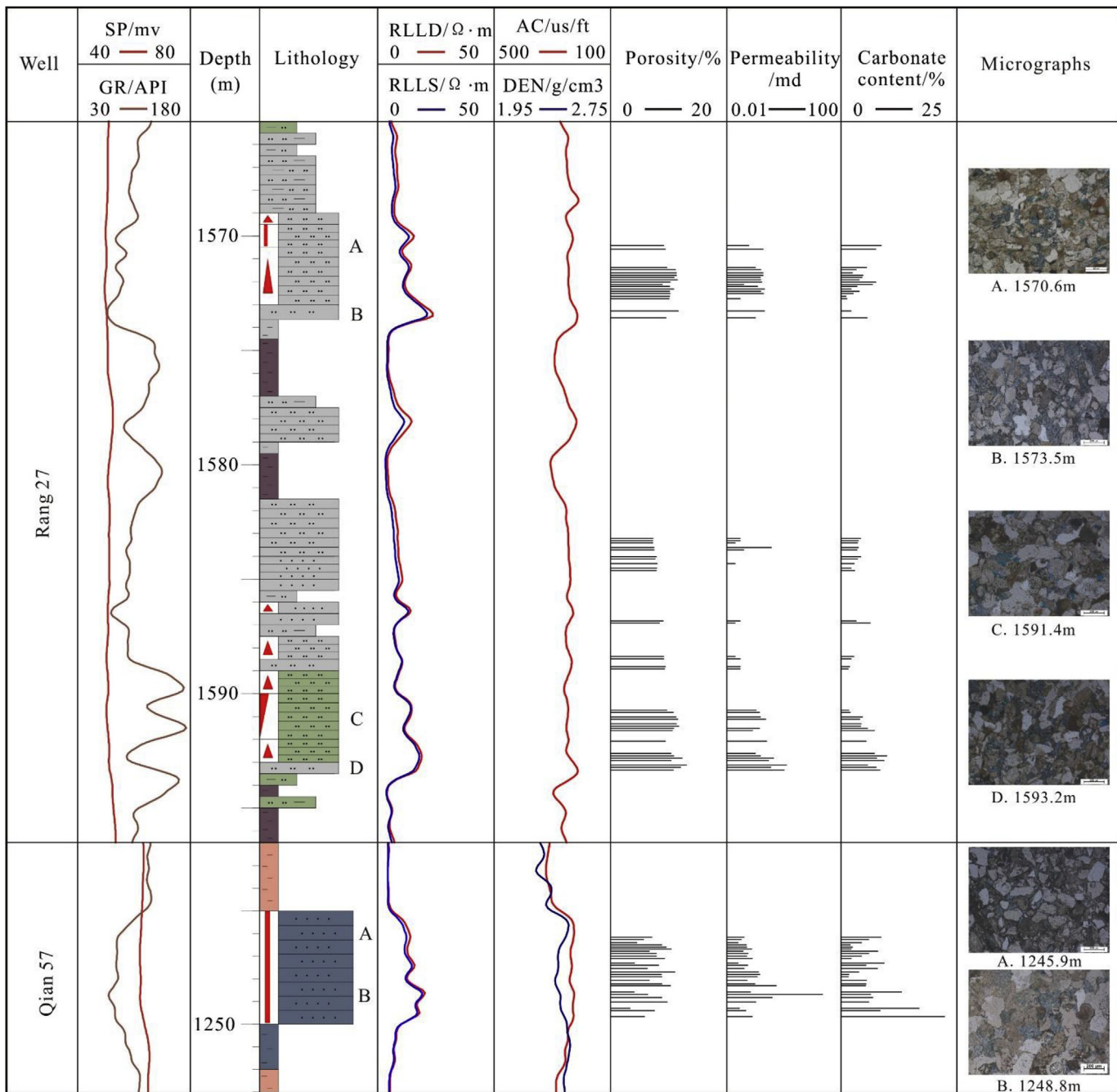


Fig. 19. Stratigraphy and reservoir quality of Well Rang 27 and Well Qian 57. Note that the carbonate cements develop more intensely along the sandstone and mudstone contacts.

abundant inorganic CO₂ contributes to the relatively more abundant carbonate cements in the TST sandstones. The (underwater) distributary channel sandstones have higher carbonate cement content than the crevasse splay or sheet sand sandstones in LST, TST and HST, respectively. Because the sandstones from crevasse splay or sheet sand have smaller grain size and higher sorting coefficient compared to the (underwater) distributary channel sandstones, which result in more intense grain stack pattern during burial and the smaller pore space for the precipitation of carbonate cements after compaction.

Core analyses and thin section observation reveals that the carbonate cements are relatively more abundant along the contact surface of sandstones and adjacent mudstones. For example, in the intervals of 1565–1595 m in well Rang 27 and 1245–1250 m in well Qian 57, the carbonate cement content is more abundant near the top and the base

of the sand body, which are close to the sandstone-mudstone contact surface, while the carbonate cement content is relatively low in the central part of the sand body (Fig. 19). Besides, the sandstones which are close to the sandstone-mudstone contact surface have relatively lower porosity and permeability, compared with the central part of the sand body. That is common in other wells throughout the study area. For sandstones within 1.0 m from the adjacent sandstone and mudstone interface, the carbonate cement decreases sharply and the abundance of carbonate cement is greater than 15%, with porosity and permeability lower than 8% and 0.1 mD, respectively (Fig. 20). For sandstones more than 3.0 m from the adjacent sandstone-mudstone contact surface, the carbonate cement content is lower than 10% and decreases gently with increasing distance, while porosity and permeability are greater than 10% and 0.1 mD respectively (Fig. 20). Therefore, the carbonate

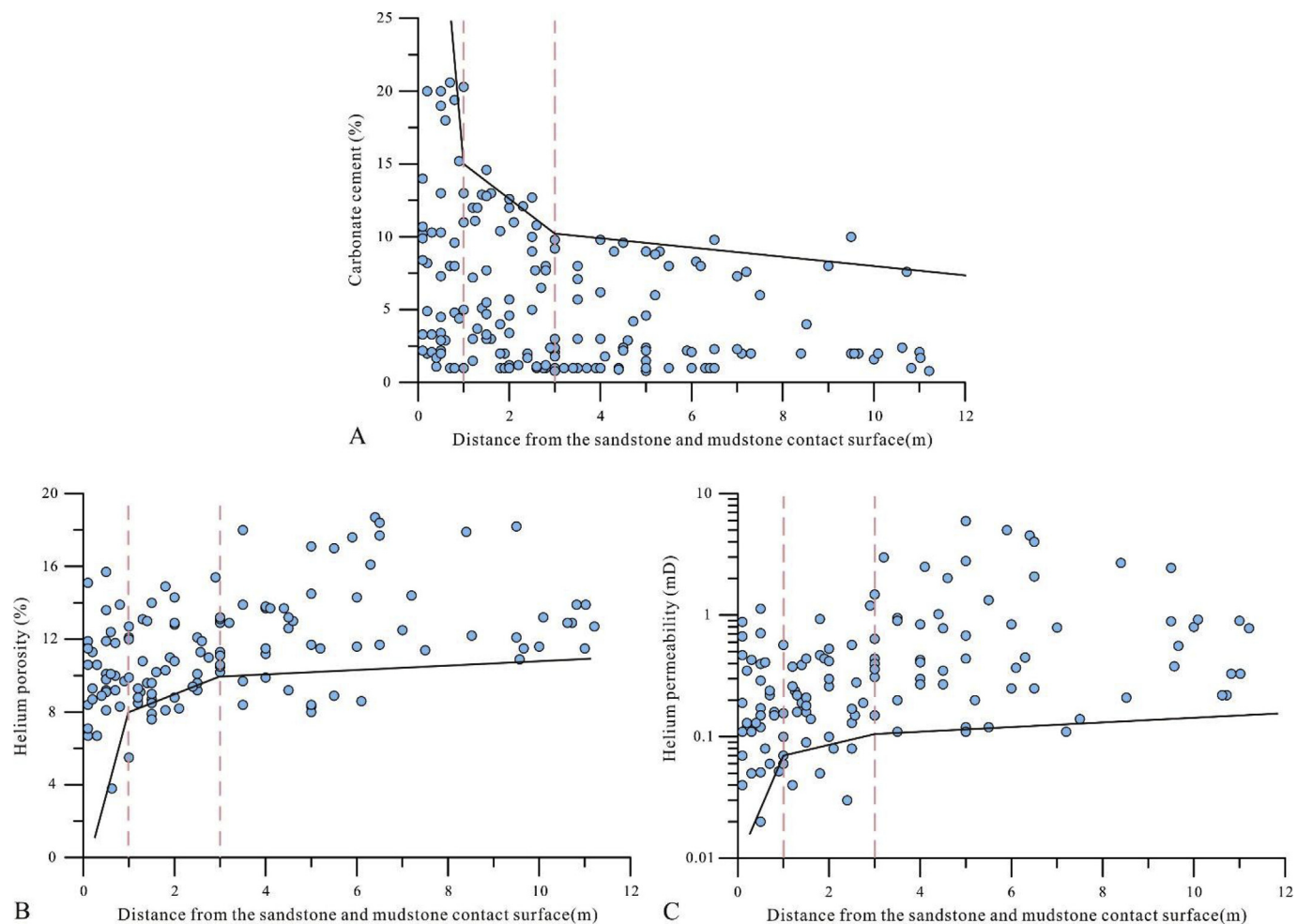


Fig. 20. Cross plots showing the relationship between the sandstone reservoir quality and the distance from the sandstone and mudrock contact surfaces. (A) Cross plot between the carbonate cement content and the distance from the sandstone and mudrock contact surfaces. (B) Cross plot between the helium porosity and the distance from the sandstone and mudrock contact surfaces. (C) Cross plot between the helium permeability and the distance from the sandstone and mudrock contact surfaces.

cement content in the sandstones were significantly affected by the distance from the adjacent sandstone-mudstone contact surface in a local scale, which also resulted in a positive correlation between the reservoir quality (porosity and permeability) and the distance from the adjacent sandstone-mudstone contact surface. As a result, the top and base of the thick sandstone bodies along the sandstone-mudstone contact surfaces commonly have low porosity and permeability due to relatively more abundant carbonate cement, while the central part of the thick sandstone bodies can retain relatively better porosity and permeability. However, thin sandstone bodies are evenly cemented by carbonate cements, which contributes to the poor reservoir quality of the sandstone reservoirs such as the LST and TST crevasse splay and HST sandstone reservoirs.

The authigenic clay minerals (4.1%–33.7%, av.13.6%), comprising mixed-layer I/S, illite, chlorite and a small amount of kaolinite, are the dominant cement in the K₁q₄ sandstones. The mixed-layer I/S, illite and chlorite are relatively common, accounting for 6%–89.9% (av.58.4%), 2.8%–73% (av.12.6%) and 0%–60% (av.21.4%) of the total clay minerals content respectively, which have different impact on porosity and permeability of the K₁q₄ sandstones in the study area.

The mixed-layer I/S is the transitional mineral of the reaction smectite-to-illite, while the illite can be transformed by smectite as mentioned above. Therefore, the abundance of mixed-layer I/S and illite even the total clay minerals content are controlled by the distribution of the eogenetic smectite which is related to the depositional

hydrodynamic force. Accompany with the rising base level, the depositional hydrodynamic force decreases from lowstand system tract to highstand system tract, which results in the increasing clay minerals (mainly smectite) content. Therefore, the mixed-layer I/S and illite are relatively more abundant in HST sandstones compared with the TST sandstones which is followed by the LST sandstones (Table 1). The mixed-layer I/S occurs mainly as grain coating cement on the grain surfaces and few amounts occurs mainly as honeycomb partially filling the pore space, which can block or decreases the intergranular pore space, and thus mainly results in the reduction in the porosity and permeability of the sandstone reservoirs (Fig. 21). Illite occurs mainly as pore-filling cement in the form of fibrous, flaky or honeycomb morphology, and sometimes bridges the pore-throat locally, which indicates that the illite is originated from the transformation of smectite and kaolinite (Moraes and De Ros, 1992; Keller et al., 1986; Morad et al., 2000). The existence of pore-filling illite can divide the intergranular pore space into complex micro-pores (Fig. 21). Therefore, the abundance of illite have significantly influence on the reservoir quality, especially the permeability (Fig. 21). The chlorite, occurring mainly as pore-lining rosette aggregates on the grain surfaces, can inhibit the quartz cementation, which can preserve the pore space result in a positive correlation with the reservoir quality (Fig. 21). According to the sources of Fe ions, the genesis of pore-lining chlorite can be divided in to three types (Tian et al., 2014): (1) the transformation of the synsedimentary grain-coating clay minerals; (2) the process of dissolution

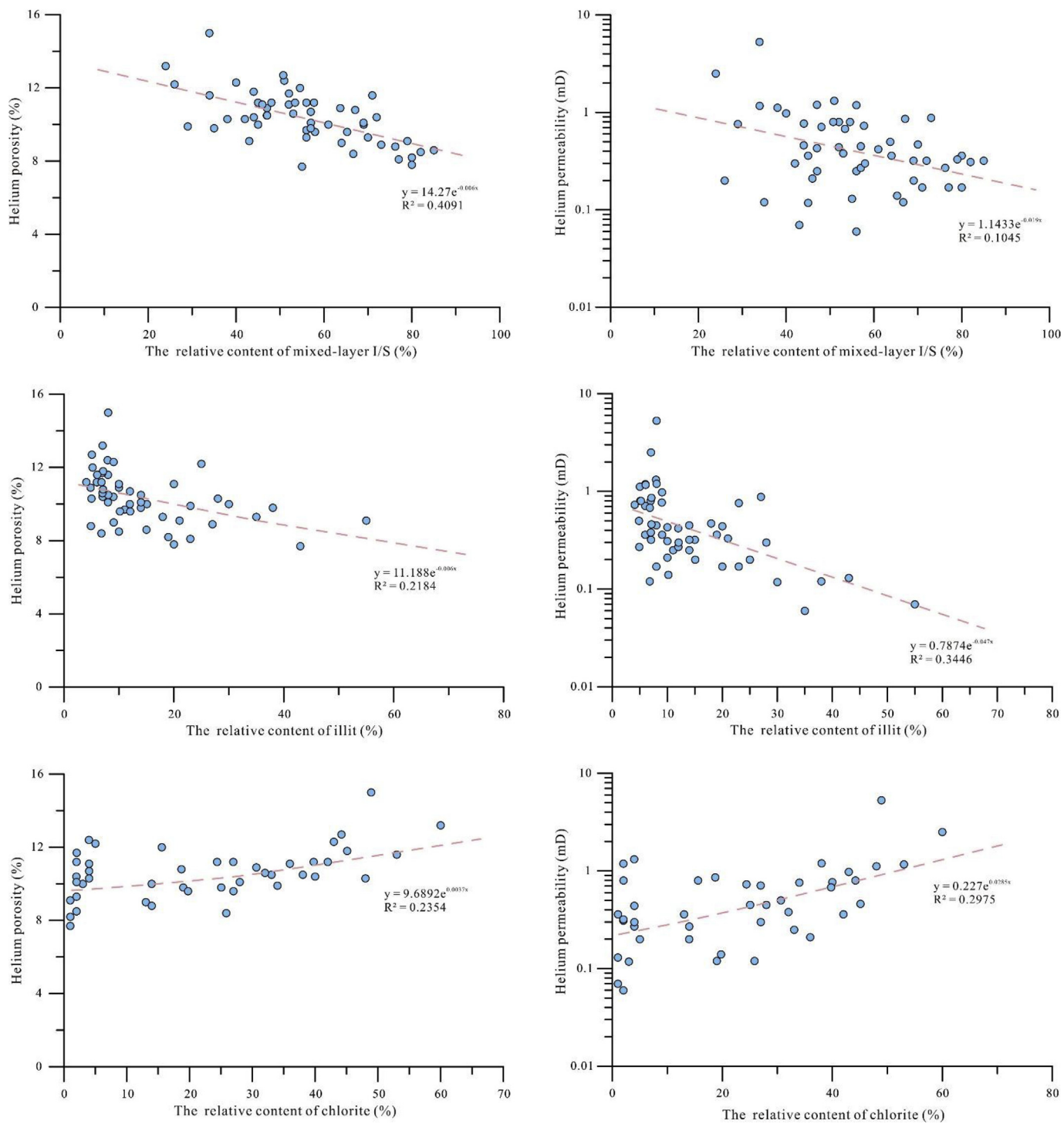


Fig. 21. Cross plots showing the relationship between the reservoir quality and different clay minerals.

and recrystallization of Fe, Mg-rich matters such as biotite and volcanic fragments; (3) the mixed process of the two types mentioned above. The absence of chlorite along the grain contacts and mixed-layer chlorite/smectite in the sandstones suggests that the chlorite precipitated after the mechanical compaction and the transformation of the synsedimentary grain-coating clay minerals is not the main source of chlorite. Therefore, the formation of chlorite is mainly related to dissolution and recrystallization of Fe, Mg-rich matters such as biotite and volcanic fragments. The chlorite is relatively more abundant in the LST and TST distributary channel sandstones compared with the HST underwater distributary channel sandstones (Table 1), because the LST and TST

distributary channel sandstones have larger grain sizes and better sorting, which can provide more space for the flow of acid fluids and facilitates the dissolution of volcanic fragments and provides more Fe, Mg-rich matters for the precipitation of chlorite.

6.3.2.3. Dissolution. According to the different sources of acid fluids, the dissolution is divided in-to organic dissolution and inorganic dissolution. However, the organic dissolution is the main mechanism caused the formation of secondary dissolution pores in the K₁q₄ sandstones due to the limited distribution range of inorganic CO₂ in the study area. Accompanied by the thermal maturation of the source

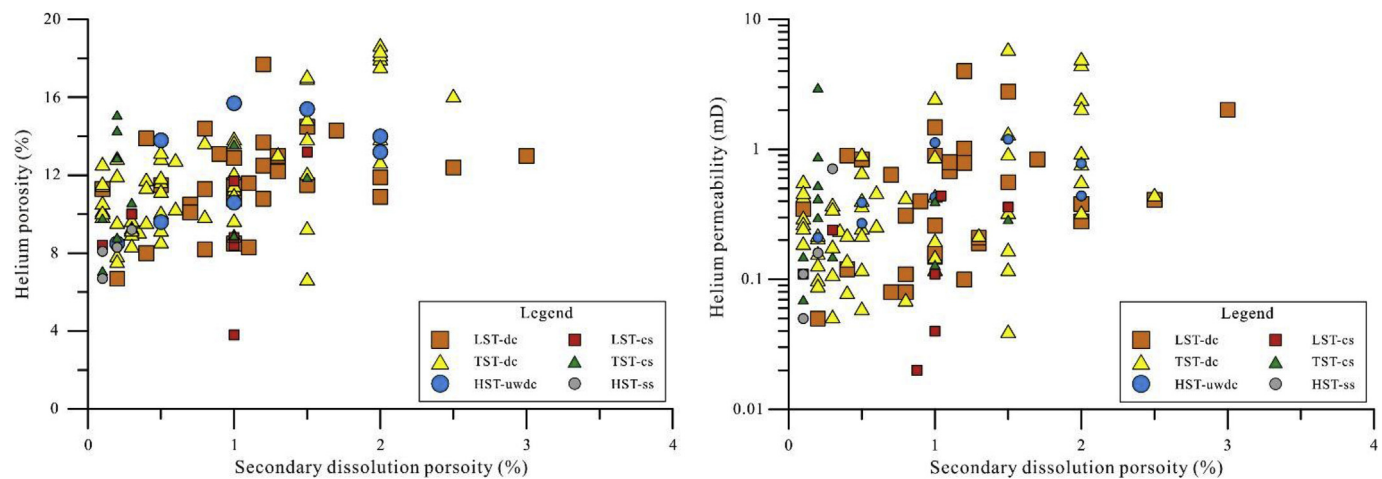


Fig. 22. Cross plots showing the relationship between the secondary dissolution porosity and reservoir quality. LST-lowstand system tract; TST-transgressive system tract; HST-highstand system tract; uwdc-underwater distributary channel; ss-sheet sand; dc-distributary channel; cs-crevasse splay.

rocks, the organic acid fluids were released into the K₁q₄ sandstones, which resulted in the dissolution of feldspars and volcanic rock fragments. Besides, the formation water turned acid during the early charging of inorganic CO₂, and the feldspars and volcanic fragments were also dissolved. The dissolution of feldspars is associated with the formation of kaolinite and quartz. The secondary dissolution porosity accounting for 10%–80% (av.31%) of the total porosity measured by the point-counting method, and the plots of dissolution porosity versus porosity and permeability respectively suggest a positive correlation between the dissolution porosity and reservoir quality (Fig. 22), which indicates that the dissolution is significant on improving the reservoir quality in the K₁q₄ sandstones. The LST and TST distributary channel and crevasse splay sandstones have the larger mean grain size than the HST underwater distributary channel and sheet sand sandstones, which contributes to the higher secondary dissolution porosity in the LST and TST sandstones than that in the HST sandstones (av.1.2%, 1.0% and 0.7% in the LST, TST and HST sandstones respectively; Fig. 22). To sum up, the LST sandstones have the best reservoir quality among the LST, TST and HST sandstones, especially the LST distributary channel sandstones, which can be ascribed to larger grain size and better sorting resulting in larger intergranular pore space after compaction, and less content of carbonate cements, illite and mixed-layer I/S, and more pore-lining chlorite and more effectively dissolution.

6.3.3. Impact of CO₂ charging on the reservoir quality

During the early charging of mantle-derived CO₂, the pore fluid environment in the sandstones turned acid which resulted in the dissolution of unstable detrital grains. Accompanied by the increasing concentration of alkali metal ions and CO₂ partial pressure in the pore fluids, the fluid environment turned alkaline - weakly acidic, and then the precipitation of dawsonite occurred. The former leads to the formation of secondary pores which can improve the reservoir quality, while the latter will destroy the reservoir quality because the dawsonite are mostly intergranular pore-filling cements. The plots of the dawsonite content versus the porosity and permeability of the dawsonite-bearing sandstones shows that the porosity and permeability increases with the increasing dawsonite content when the dawsonite content is less than 5%; while the reservoir quality decreases with the increasing dawsonite content when the dawsonite content is greater than 5% (Fig. 23). The dawsonite content ranges from 1% to 10% in the dawsonite-bearing sandstone samples, and the dawsonite content of most dawsonite-bearing sandstone samples is greater than 5%. On the whole, the charging of CO₂ is harmful to the reservoir quality of the K₁q₄ sandstones in the study area.

7. Conclusions

The K₁q₄ sandstones in the southern Fuxin uplift zone were mostly deposited in distributary channels and crevasse splays of a delta plain within the LST and TST, and underwater distributary channels and sheet sands of a delta front within the HST. The K₁q₄ sandstones, silt to medium grained, medium to well sorted, and mostly lithic arkoses and feldspathic litharenites, have undergone significantly diagenetic alterations, such as compaction, quartz cementation, unstable grains (feldspar and volcanic fragments) dissolution, carbonate cementation and clay minerals cementation.

The reservoir quality of the K₁q₄ sandstones are poor with low porosity and permeability, showing variations among the different system tracts and depositional facies, and are influenced by the charging of CO₂ and controlled by the combination of sequence stratigraphy, depositional facies and diagenesis.

The carbon sources of carbonate cements was probably external mixed sources. The carbon source of dawsonite was mostly provided by the inorganic CO₂ originated from mantle-derived magma, and the adjacent mudstones and the overlying source rocks are possibly another carbon source. The ferrocalcite and ankerite mainly derived from the adjacent mudstones and the overlying source rocks and the inorganic CO₂ may also participated the precipitation process.

The sequence stratigraphic framework exerted a significant control on the depositional setting, resulting in the variations in depositional environments among the LST, TST and HST sandstones. The sandstones with high reservoir quality are mostly deposited in high energy environments, including the (underwater) distributary channel sandstones, especially the LST distributary channel sandstones with the best reservoir quality among the LST, TST and HST sandstones, which can be ascribed to larger grain size and better sorting resulting in larger intergranular pore space after compaction, and less content of carbonate cements, illite and mixed-layer I/S, and more pore-lining chlorite and more effectively dissolution. The poor reservoir quality of sandstones from crevasse splay and sheet sand is due to the small grain size and bad sorting which resulted in extensive compaction and the resulting weak dissolution.

The charging of CO₂ has dual impact on the reservoir quality of the K₁q₄ sandstones. The CO₂ charging can induce the dissolution of unstable detrital grains and the precipitation of dawsonite, the former create new secondary pore space, while the latter occupy the intergranular pore space. The CO₂ charging is harmful to the reservoir quality when the dawsonite content exceeds a threshold of 5%.

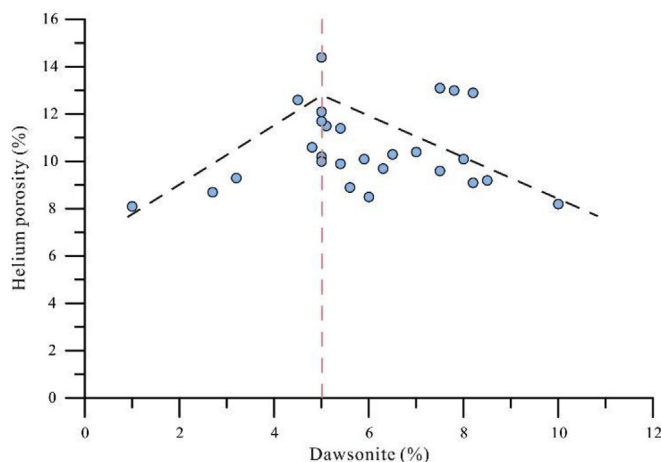


Fig. 23. Cross-plots showing the relationship between dawsonite content and helium porosity and permeability.

Acknowledgements

We thank PetroChina Jilin Oilfield Company for their support in collecting data and for granting permission to publish the results. The research was co-funded by the National Science and Technology Major Project of China (No. 2017ZX05009-001), and the Fundamental Research Funds for the Central Universities (No. 15CX06012A).

References

- Amel, H., Jafarian, A., Husinec, A., Koeshidayatullah, A., Swennen, R., 2015. Microfacies, depositional environment and diagenetic evolution controls on the reservoir quality of the permian upper dalan formation, kish gas field, zagros basin. *Mar. Petrol. Geol.* 67, 57–71.
- Boles, J.R., Franks, S.G., 1979. Clay diagenesis in Wilcox sandstones of southwest Texas: implications of smectite diagenesis on sandstone cementation. *J. Sediment. Petrol.* 49, 55–70.
- Curtis, C.D., 1978. Possible links between sandstone diagenesis and depth-related geochemical reactions occurring in enclosing mudstones. *J. Geol. Soc.* 135, 107–117.
- Dutton, S.P., 2008. Calcite cement in Permian deep-water sandstones, Delaware Basin, west Texas: origin, distribution, and effect on reservoir properties. *AAPG Bull.* 92, 765–787.
- Dutton, P.S., Loucks, G.R., 2010. Diagenetic controls on evolution of porosity and permeability in lower Tertiary Wilcox sandstones from shallow to ultradeep (200–6700 m) burial, Gulf of Mexico Basin, U.S.A. *Mar. Petrol. Geol.* 27, 69–81.
- Feng, C., Shan, Q., Shi, W., Zhu, S., 2013. Reservoirs heterogeneity and its control on remaining oil distribution of K1q4, Fuyu Oilfield. *Journal of China University of Petroleum* 37, 1–7.
- Feng, Z., Jia, C., Xie, X., Zhang, S., Feng, Z., Cross, T., 2010. Tectonostratigraphic units and stratigraphic sequences of the nonmarine Songliao basin, northeast China. *Basin Res.* 22, 79–95.
- Folk, R.L., 1974. Petrology of Sedimentary Rocks. Hemphill, Austin, Texas, pp. 182.
- Friedman, I., O'Neil, J.R., 1977. Composition of stable isotopic fractionation factors of geochemical interest. In: Fleisher, M. (Ed.), Data of Geochemistry, 6th U.S. Geological Survey: Professional Paper, vol. 440. pp. 1–12.
- Gao, Y., Liu, L., Yang, H., You, L., Liu, N., 2007. Characteristics and origin of dawsonite in Gudian carbon dioxide gas field of Songliao Basin. *Acta PetroleiSin* 28, 62–67.
- Hammer, E., Mørk, M.B.E., Næss, A., 2010. Facies controls on the distribution of diagenesis and compaction in fluvial-deltaic deposits. *Mar. Petrol. Geol.* 27, 1737–1751.
- Heritsch, H., 1975. Dawsonite as a product of low- hydrothermal transformation of a volcanic breccia from a borehole in eastern Styria (Austria): neus Jahrbuch Fur Mineralogie. Monatshefte 8, 360–368.
- Houseknecht, W.D., 1987. Assessing the relative importance of compaction processes and cementation to reduction of porosity in sandstones. *AAPG (Am. Assoc. Pet. Geol.) Bull.* 71, 633–642.
- Hu, X., Bao, Z., Na, W., Zhou, X., 2008. Sedimentary facies of the fourth member of Quantou formation in fuyu oilfield, the south Songliao basin. *Oil Gas Geol.* 29, 334–341.
- Irwin, H., Curtis, C., Coleman, M., 1977. Isotopic evidence for source of diagenetic carbonates formed during burial of organic-rich sediments. *Nature* 269, 209–213.
- Karim, A., Piper, P.G., Piper, J.M.D., 2010. Controls on diagenesis of lower cretaceous reservoir sandstones in the western sable subbasin, offshore nova scotia. *Sediment. Geol.* 224, 65–83.
- Kim, J.C., Lee, Y.I., Hisada, K., 2007. Depositional and compositional controls on sandstone diagenesis, the tectori group (middle jurassic-early cretaceous), central Japan. *Sediment. Geol.* 195, 183–202.
- Keller, W.D., Reynolds, R.C., Inoue, A., 1986. Morphology of clay minerals in the smectite-to-illite conversion series by scanning electron microscopy. *Clay Clay Miner.* 34, 187–197.
- Lan, C., Yang, M., Zhang, Y., 2016. Impact of sequence stratigraphy, depositional facies and diagenesis on reservoir quality: A case study on the Pennsylvanian Taiyuan sandstones, northeastern Ordos Basin, China. *Mar. Petrol. Geol.* 69, 216–230.
- Li, Y., Yu, K., Jiang, Y., Chen, S., Zhang, E., Song, Y., 2007. N. In: A New Explanation for the Stratigraphical Sequence of Quan 4th Member of the Fuyu Oil Layer in the Songliao Bas, vol. 37. Periodical of Ocean University of China, pp. 977–982.
- Li, D., Dong, C., Lin, C., Ren, L., Jiang, T., Tang, Z., 2013. Control factors on tight sandstone reservoirs below source rocks in the Rangzijing slope zone of southern Songliao Basin, East China. *Petrol. Explor. Dev.* 40, 692–700.
- Liu, L., Hou, Q., Liu, N., Yang, H., Li, F., Yu, Z., 2011. Charging time sequence of mantle CO₂and hydrocarbon in southern Songliao Basin: an evidence from dawsonite-bearing sandstones. *Oil Gas Geol.* 32, 873–881.
- Lundegard, P., 1992. Sandstone porosity loss - a “big picture” view of the importance of compaction. *J. Sediment. Petrol.* 62, 250–260.
- Marchand, A.M., Apps, G., Li, W., Rotzien, J.R., 2015. Depositional processes and impact on reservoir quality in deepwater Paleogene reservoirs, US Gulf of Mexico. *AAPG (Am. Assoc. Pet. Geol.) Bull.* 99, 1635–1648.
- Matthews, A., Katz, A., 1977. Oxygen isotope fractionation during the dolomitization. *Geochem. Cosmochim. Acta* 41, 1431–1438.
- McHargue, T.R., Price, R.C., 1982. Dolomite from clay in argillaceous limestones or shale associated marine carbonates. *J. Sediment. Petrol.* 52, 873–886.
- Morad, S., Ketzer, J.M., Deros, L.F., 2000. Spatial and temporal distribution of diagenetic alterations in siliciclastic rocks, implications for mass transfer in sedimentary basins. *Sedimentology* 47 (Suppl. 1), 95–120.
- Morad, S., Al-Ramadan, K., Ketzer, J.M., De Ros, L.F., 2010. The impact of diagenesis on the heterogeneity of sandstone reservoirs: a review of the role of depositional facies and sequence stratigraphy. *AAPG (Am. Assoc. Pet. Geol.) Bull.* 94, 1267–1309.
- Moraes, M.A.S., De Ros, L.F., 1992. Depositional infiltrated and authigenic clays in fluvial sandstones of the Jurassic Sergi Formation, Reconcavo Basin, northeastern Brazil. In: In: Houseknecht, D.W., Pittman, D.E. (Eds.), Origin, Diagenesis, and Petrophysics of Clay Minerals in Sandstones, vol. 47. SEPM, Society for Sedimentary Geology, Tulsa, OK, United States, pp. 197–208.
- Qu, X.Y., Liu, L., Gao, Y.Q., Liu, N., Peng, X.L., 2008. Characteristics and stability analysis of dawsonite in sandstone. *Geol. Rev.* 54, 838–844 (in Chinese with English abstract).
- Qu, X., Liu, L., Gao, Y.Q., Liu, N., Li, F.L., Liu, H.Y., 2010. Geology record of mantle derived magma to genetic CO₂ gas in the northeastern China. *Acta Pet. Sin.* 31, 61–67 (in Chinese, with English Abstr.).
- Qu, X., Chen, X., Yu, M., Liu, L., 2016. Mineral dating of mantle – derived CO₂ charging and its application in the southern Songliao Basin, China. *Appl. Geochem.* 68, 19–28.
- Tian, J., Jian, Y., Zhang, Q., 2014. The pore-lining chlorite formation mechanism and its contribution to reservoir quality. *Journal of Jilin University* 44, 741–748.
- Trendell, A.M., Atchley, S.C., Nordt, L.C., 2012. Depositional and diagenetic controls on reservoir attributes within a fluvial outcrop analog: upper triassic sonsela member of the chinle formation, petrified forest national park, Arizona. *AAPG (Am. Assoc. Pet. Geol.) Bull.* 96, 679–707.
- Wang, P., Xie, X., Frank, M., Ren, Y., Zhu, D., Sun, X., 2007. The cretaceous Songliao basin: volcanogenic succession, sedimentary sequence and tectonic evolution, ne China. *Acta Geologica Sinica (English Edition)* 81, 1002–1011.
- Wei, H.H., Liu, J.L., Meng, Q.R., 2010. Structural and sedimentary evolution of the southern Songliao Basin, northeast China, and implications for hydrocarbon prospectivity. *AAPG (Am. Assoc. Pet. Geol.) Bull.* 94, 531–564.
- Worden, R.H., 2006. Dawsonite cement in the Triassic Lam Formation, Shabwa Basin, Yemen: a natural analogue for a potential mineral product of subsurface CO₂ storage for greenhouse gas reduction. *Mar. Petrol. Geol.* 23, 61–77.
- Xiong, F., Shi, G., Sun, Y., Sun, Y., 2008. Research on sedimentary microfacies of fourth section of Quantou formation in liangjing gudian area of Songliao basin. *Acta Sci. Nauralium Univ. Pekin.* 44, 185–192.
- Xi, K., Cao, Y., Jaren, J., Zhu, R., Bjørlykke, K., Zhang, X., Cai, L., Hellevang, H., 2015a. Quartz cement and its origin in tight sandstone reservoirs of the Cretaceous Quantou formation in the southern Songliao Basin, China. *Mar. Petrol. Geol.* 66, 748–763.

- Xi, K., Cao, Y., Jahren, J., Zhu, R., Bjørlykke, K., Haile, B.G., Zheng, L., Hellevang, H., 2015b. Diagenesis and reservoir quality of the lower cretaceous Quantou formation tight sandstones in the southern Songliao basin, China. *Sediment. Geol.* 330, 90–107.
- Yang, R., Fan, A., Han, Z., Wang, X., 2012. Diagenesis and porosity evolution of sandstone reservoirs in the East II part of Sulige gas field, Ordos Basin. *International Journal of Mining Science and Technology* 22, 311–316.
- Yu, M., Liu, L., Yu, Z.C., Liu, N., Yang, H.D., Qu, X.Y., 2014. Dawsonite fixation of mantle CO₂ in the cretaceous Songliao Basin, Northeast China: a natural analogue for CO₂ mineral trapping in oilfields. *Int. Geol. Rev.* 56, 1792–1812.
- Yuan, G., Gluyas, J., Cao, Y., Oxtoby, H.N., Jia, Z., Wang, Y., 2015. Diagenesis and reservoir quality evolution of the eocene sandstones in the northern dongying sag, bohai bay basin, east China. *Mar. Petrol. Geol.* 22, 77–89.
- Zhang, Y., Piper, P.G., Piper, J.W.D., 2015. How sandstone porosity and permeability vary with diagenetic minerals in the Scotian Basin, offshore eastern Canada: implications for reservoir quality. *Mar. Petrol. Geol.* 63, 28–45.
- Zou, C., Tao, S., Zhang, Y., 2007. Study on the accumulation time of lithologic reservoir in southern Songliao basin and significance in exploration. *Chin. Sci. Bull.* 52, 2319–2329.